ADVANCED ELECTRIC PROPULSION RESEARCH

PREPARED FOR

NATIONAL AERONAUTICS AND SPACE ADMINISTRATION

GRANT NGR06-002-032

GPO PRICE $ ____________

CFSTI PRICE(S) $ ____________

Hard copy (HC) 3.00

Microfiche (MF) .65

ff 653 July 65

REPORT NO. 6

SPACE PROPULSION PROGRAM
ENERGY CONVERSION PROGRAM
COLLEGE OF ENGINEERING
COLORADO STATE UNIVERSITY
FORT COLLINS, COLORADO

MER 67-68WRM-9

ANNUAL REPORT

For the period January 1, 1967 to December 31, 1967

ADVANCED ELECTRIC PROPULSION RESEARCH

Prepared for

NATIONAL AERONAUTICS AND SPACE ADMINISTRATION

December 1967

Grant NGR06-002-032

Technical Management

George Pfannebecker
Nuclear Electric Systems Division
Office of Advanced Research Technology
NASA Headquarters
Washington, D.C. 20546

Prepared by: William R. Mickelsen

William R. Mickelsen, principal investigator
Professor of Mechanical Engineering
and Professor of Electrical Engineering
Engineering Center
Colorado State University
Fort Collins, Colorado 80521

CONTENTS

SUMMARY

Approximate methods for electric propulsion mission analysis were investigated. A characteristic length has been found that offers excellent correlation between low-thrust trajectories with various types of thrust programs. Good correlation was also found between low-thrust trajectories and impulsive thrust trajectories of the direct type.

General relativity has been reviewed for possible applications to space propulsion. Although this review was cursory, several aspects of general relativity were found that might possibly be of interest.

Volume ion production power losses in mercury-and cesium-bombardment thrusters were evaluated using a general-atom theory based on the Gryzinski expressions. The results of this analysis predict that mercury thrusters will have about 2.5 times as much volume ion power loss as that in cesium-bombardment thrusters.

Equipment has been fabricated and assembled for the measurement of neutral-atom energy in a mercury-bombardment thruster. The experiment is nearly operational.

Heat addition to supersonic nozzle flow has been treated with a one-dimensional flow analysis with lithium as the fluid. The flow velocity can be increased several fold in theory, and the mode of heat addition has a marked effect on nozzle area ratio. Further work is being done to find the optimum mode of heat addition.

Electrostatic spraying of a number of biowaste-type liquids has been studied experimentally. There has been success with some liquids, but freezing at the needle tip has been a problem with other liquids.

APPROXIMATE METHODS IN ELECTRIC PROPULSION MISSION ANALYSIS*

by William R. Mickelsen**

Colorado State University
Fort Collins, Colorado

ABSTRACT

A definite need exists for approximate, simple, fast and flexible methods for preliminary analysis of electric propulsion missions. Methods are presented which serve these ends, and provide a straightforward technique for the determination of the effects of system components on mission performance. These approximate techniques utilize a combination of existing trajectory and mission analysis techniques, such as impulsive thrust analysis, characteristic length, and low-thrust mission characteristics. Practical constraints associated with electric propulsion systems are included throughout the analysis.

These methods have been compared with more exact solutions of the Mars orbiter-lander and the Jupiter fly-by missions. Power profiles from more exact solutions, linearized profiles, and profiles deduced from impulsive-thrust trajectories, were used as inputs to the approximate analysis. The approximate methods provided final mass fractions within about ten percent of the more exact analyses.

The good results obtained with the approximate methods in a wide variety of mission profiles has established confidence in the approximate methods. It appears that these methods can be used for preliminary screening of mission profiles, to be followed by the more exact analyses.

INTRODUCTION

A considerable amount of work has been done in low-thrust trajectory analysis. Essentially all of this work has been with the patched-conic approximation, but has provided digital computer

---

* done under NASA Grant NGR06-002-032, Electric Thruster Systems, OART.

**Associate Fellow, AIAA. Professor of Mechanical Engineering and Electrical Engineering.

programs and trajectory data with about 1-2% accuracy. Digital programs of this kind require considerable time between definition of input and receipt of legible output. In addition, the mission analyst is not provided conveniently with an intimate knowledge of the variation of all parameters throughout the mission profile. More complex trajectory analysis such as optimized three-dimensional n-body programs with 0.1% accuracy, or double-precision three-dimensional n-body full-parameter-optimization programs, will provide even less insight, flexibility, and speed for the mission analyst. A simple, fast, and flexible analysis method is needed for preliminary mission analysis.

An ideal program, or method, for those working in electric propulsion should have certain characteristics. In the interest of providing these characteristics, accuracy could be sacrificed; for example an accuracy of 10% in payload would be adequate. The method should be analytic if possible, although some graphical interpolation would be acceptable. If the method were entirely analytic, then the ease in understanding would result in ease of modification of the method. The feature of easy modification would be of great importance in analyzing missions with unusual profiles.

An essential characteristic is that the method be independent from the accurate methods. Some simple and fast methods have been developed, but these depend on results obtained from the accurate trajectory analyses. To provide true flexibility, only the fundamental properties of the solar system, and simple characteristics of impulsive thrust trajectories should be necessary for evaluation of any mission profile.

Approximate optimization of the mission profile should be straightforward, and should provide a direct insight into the relative merits of various trade-offs. This feature would make it possible to compare various electric propulsion systems for each particular mission profile, or to compare various combinations of propulsion systems. A straightforward optimization procedure would also provide means for evaluating the performances of each component in the electric propulsion system.

The methods described here are intended to fulfill these needs and requirements.

THE CHARACTERISTIC-LENGTH APPROXIMATION

The Zola characteristic length[1] provides a means for using impulsive-thrust trajectory characteristics in estimating low-thrust missions. Because of this convenient relationship to the readily available impulsive-thrust trajectory information, and because of the conceptual simplicity of characteristic length, it is used throughout the approximate methods discussed in this paper.

Characteristic length is defined as the distance that would be traveled by the vehicle in field-free space. For example, the distance ΔL travelled in time t_1 is simply:

$$\Delta L \equiv \int_0^{t_1} V \, dt \qquad (1)$$

where V is the instantaneous speed along a rectilinear path. Speed V is simply the integral of instantaneous acceleration:

$$V \equiv \int_0^{t} a \, d\tau \qquad (2)$$

where the instantaneous acceleration a is:

$$a \equiv \frac{F}{M} \qquad (3)$$

Thrust F may vary with time, and vehicle mass M decreases with time. It must be noted that rectilinear motion is assumed.

In field-free space, it is clear that an infinite variety of thrust programs could be used to propel a vehicle the same length L. If two thrust programs result in the same characteristic length, then those programs are equivalent in the sense that either one will accomplish the mission. Stated in another way, a given mission has a characteristic length which is invariant for all thrust programs satisfying the mission conditions.

In applying the characteristic length to missions in gravitational fields, it is assumed that the characteristic length is still invariant for all thrust programs. If a particular mission, say, a 230-day Mars orbiter, requires a hyperbolic velocity V_1 at Earth and an approach hyperbolic velocity V_2 at Mars, then the characteristic length L for the mission is:

$$L = (V_1 + V_2)\ t/2 \tag{4}$$

The assumption of invariant length implies that low-thrust vehicles must have thrust profiles such that the summation of the lengths ΔL must be equal to the characteristic length:

$$L = \sum_{i=1}^{n} \Delta L_i \tag{5}$$

Further description of the characteristic length is best accomplished with the example missions treated in the following sections.

SOLAR-ELECTRIC POWER PROFILES

Calculation of the low-thrust V and ΔL_i requires definition of the variation of instantaneous thrust-acceleration with time, as indicated by equations (1) and (2).

A general expression for instantaneous thrust-acceleration is:

$$a = \frac{F}{M} = \frac{F}{M_o - \dot{m}t} = \frac{1}{\frac{1}{F/M_o} - \frac{t}{v_{j,eff}}} = \frac{1}{\frac{1}{a_o(P/P_o)} - \frac{t}{v_{j,eff}}} \tag{6}$$

where a_o is the thrust-acceleration at the beginning of the mission, $v_{j,eff} = g_c I$, I is specific impulse, P/P_o is the variation of power with time, and P_o is power at 1 AU.

Electric propulsion systems presently envisioned must operate at constant specific impulse throughout a mission.

Solar-electric power varies with distance from the Sun, both because of the dependence of solar flux intensity on distance from the Sun, and because of the dependence of solar-cell output on cell temperature. Solar-array power output has been calculated and is listed[2] as a function of radius from the sun. However, distance from the Sun as a function of time is not known a priori for the low-thrust trajectory, so resort must be made to an approximation.

Distance from the Sun can be computed accurately for impulsive thrust trajectories from simple formula. By combining this impulsive-thrust trajectory information with the solar-array power information;

the solar-array power can be calculated as a function of time for vehicles that are on impulsive-thrust trajectories. Power profiles for out-bound trajectories were determined by this method, and are shown in Figure 1 for a range of hyperbolic departure speeds. The hyperbolic speed V_H is defined as the speed of the vehicle with respect to Earth after leaving the Earth's gravitation field. For the profiles shown in Figure 1, V_H was assumed to be tangent to the (mean) circular orbit of Earth.

If a solar-electric vehicle is launched with a particular value of V_H, say, 2 km/sec, then it is clear that as the low-thrust-acceleration continues, the power will decrease more rapidly than indicated by the impulsive-thrust (coasting) trajectory power profile shown in Figure 1. During some time interval $\Delta t'$, the low-thrust-acceleration will have propelled the vehicle through a characteristic length $\Delta L'$, so the vehicle will have reached a distance from the Sun approximately equal to the distance it would have reached by coasting from an initial hyperbolic speed V_H'. This equivalence of characteristic length is expressed by:

$$\Delta L' = (V_H' - V_H)\ \Delta t' \qquad (7)$$

If $\Delta L'$ can be estimated for a given time interval $\Delta t'$, then V_H' can be calculated from equation (7), and this estimate provides a point on a V_H' curve in Figure 1 at the time $\Delta t'$. By this means, a power profile can be estimated for a given thrust-acceleration and specific impulse.

APPROXIMATELY LINEAR POWER PROFILES

At Mars, the power ratio is $P/P_o = 0.47$ and at Jupiter, $P/P_o = 0.05$. For a 230-day Mars mission, a linear power profile falls between the impulsive-thrust profiles for a V_H of 2 and 4 km/sec, as shown in Figure 2. This implies that a linear profile could be assumed for a 230-day Mars mission with a V_H of about 2 km/sec. Similarly, a linear power profile appears to be a reasonable assumption for a 600-day Jupiter mission with a V_H of about 1 km/sec.

Field-free rectilinear velocities V, and lengths ΔL have been calculated[3] for linear power profiles over a wide range of initial thrust accelerations a_o, for Earth-Mars and Earth-Jupiter missions. Examples of these calculations are shown in Figures 3 and 6. These calculations can be used to analyze Mars and Jupiter solar-electric missions.

MARS ORBITER-LANDER SOLAR-ELECTRIC MISSION

Mars orbiter-lander missions have been analyzed[2] with a precision digital-computer program, so it is of interest to compare those precision results with estimates obtained with the present approximate methods. A particular mission profile from the precision analyses is shown in Figure 7. This mission is for the following specifications:

optimum lauch date in 1971
mission time, $t = 231$ days
$C_3 = 4.23\ \text{km}^2/\text{sec}^2$ (ie, $V_H = 2.06$ km/sec)
specific impulse, $I = 4000$ sec
initial mass, $M_o = 2520$ kg
thruster efficiency, $\eta_{th} = 0.64$
power-conditioning efficiency, $\eta_c = 0.92$
continuous forward thrust

Total length ΣL for the low-thrust trajectory is simply the sum of ΔL_1 and ΔL_2 as illustrated in Figure 7. The length ΔL_1 is the product of the hyperbolic departure velocity V_H and the mission time t. The length ΔL_2 can be read from Figure 4 for a range of initial thrust-acceleration a_o. Then the length summation $\Sigma\Delta L$ can be plotted as a function of initial thrust-acceleration a_o as shown in Figure 8.

Characteristic length L for this mission can be calculated from equation (4). The velocities V_1 and V_2 are found from the literature[4], and the length is $L = 6.1 \times 10^{10}$ meters. As shown in Figure 8, the thrust-acceleration that satisfies the characteristic length L is $a_o = 1.22 \times 10^{-4}\ \text{m/sec}^2$. Vehicle parameters such as power level and propellant required can be calculated from the value of a_o (e.g., the average mass-flow rate can be found from the average power ratio). Vehicle parameters determined from this approximate method are compared below with those from the precision program:

	precision program[2]	approximate method
solar-array power, kwe	9.6	9.7
propellant mass, kg	112	115

Agreement is good between these results.

JUPITER FLY-BY SOLAR-ELECTRIC MISSIONS

Mission with Linear Power Profile

A Jupiter fly-by mission with a complex thrust program has been analyzed[2] with a precision digital computer program. This mission profile is illustrated in Figure 9, and has the following specifications:

launch date, 1 Dec 1973
mission time, $t = 900$ days
reverse hyperbolic speed, $V_H = 1.1$ km/sec
specific impulse, $I = 3500$ sec
initial mass, $M_o = 1185$ kg
thruster efficiency, $\eta_{th} = 0.59$
power-conditioning efficiency, $\eta_c = 0.92$
reverse low thrust, $t_1 = 20$ days
leave vicinity of Earth orbit, $t_2 = 140$ days
thrust termination, $t^* = 540$ days

Since the vehicle remains in the vicinity of Earth for 140 days, the reverse and forward low-thrust values of V can be calculated from equations (2) and (6) with $P/P_o = 1$. Then starting at t_2, the speed V^* can be found from Figure 5, and the length ΔL_2 from Figure 6. The other lengths, ΔL_1 and ΔL_3, can be calculated simply as products of speeds and time intervals. The resulting length summation is shown in Figure 10 for a range of initial thrust-accelerations a_o. Characteristic length L was determined from the literature[5] for impulsive-thrust trajectories beginning at the time when $V = 0$ for each assumed value of a_o, so L is also a function of initial thrust-acceleration. Solar-array power calculated from the value of $a_o = 4.78 \times 10^{-4}$ m/sec^2 shown in Figure 10, is $P = 18$ kwe. This is in close agreement with the value of 17 kwe found in the precision analysis[2].

Mission with Non-Linear Power Profile

The approximate methods have been tested in a mission case where the power profile cannot be assumed to be a linear function of time. The sample mission used has been analyzed with precision digital-computer programs[6,7]. A set of specifications for this mission are:

optimum launch date in 1976
mission time, $t = 600$ days
$V_H = 4000$ m/sec
specific impulse, $I = 3230$ sec.
tankage, $k = 0.1$
propulsion system specific mass, $\alpha_{ps} = 30$ kg/kwe
initial mass, $M_o = 700$ kg
thruster and power conditioning efficiency, $\eta_{th} \cdot \eta_c = 0.535$

By inspection of Figure 2, it is evident that with a $V_H = 4$ km/sec, the power profile cannot be approximated with a linear relation.

Characteristic length was used in the present analysis to generate power profiles for the 600-day Jupiter mission. For example, if $a_o = 0.0003$ m/sec^2, then equation (7) is satisfied for $V_H' = 6$ km/sec when $\Delta t' = 175$ days, by inspection of Figure 6. This implies that at $t = 175$ days, the power profile for $a_o = 0.0003$ m/sec^2 should pass through the curve for $V_H = 6$ km/sec (Figure 1), ie, $P/P_o = 0.33$ at $t = 175$ days. In this manner, the power profiles were estimated by use of Figures 1 and 6, with the results shown in Figure 11. For the assumptions made herein, these profiles are universal for 600-day Earth-Jupiter heliocentric transfers.

With the power-profiles shown in Figure 11, it is a simple matter to calculate field-free rectilinear speeds V and length ΔL_2 for the mission profile shown in Figure 12. From these calculations, the length summation $\Sigma \Delta L$ can be obtained for ranges of initial thrust-acceleration a_o and propulsion time t^*. These results are shown in Figure 13.

For the optimum launch date in 1976, the characteristic length calculated from impulsive thrust information[5] is $L = 48.5 \times 10^{10}$ meter. With this characteristic length, the initial thrust-acceleration was determined from Figure 13 for the range of propulsion times t^*. Then the power and propellant requirements were determined from a_o, I, and M_o. The propellant calculations included a 10% tankage, and an average mass-flow rate found by inspection of the power profiles.

Payload was then calculated for the range of propulsion times, with the results shown in Figure 14. For comparison, the precision digital-computer program[6] yields a payload of 181 kg at about 440 days propulsion time. This agreement is good.

SUMMARY OF GENERAL METHOD

The approximate methods described in the previous sections are applicable to constant specific impulse, solar-electric, heliocentric trajectories. To apply these methods, it is necessary to have information about the analogous impulsive-thrust trajectories; and it is convenient to have certain universal graphs of V and ΔL for low-thrust trajectories. A typical application of the approximate methods is outlined below.

(a) define the mission in general, e.g. constant specific impulse, solar-electric, Earth-Jupiter

(b) prepare plots of P/P_o versus t for several values of V_H, for outbound impulsive-thrust trajectories (these impulsive-thrust trajectories may be based upon any desired mathematical model ranging from two-body, two-dimensional up through n-body, three dimensional; the implication is that the accuracy of this approximate method depends on the degree of sophistication of the impulsive trajectory model.)

(c) prepare plots of V and of ΔL versus t for several values of a_o and of trip time, for linear power profiles (i.e., $P/P_o = -kt$)

(d) prepare universal plots of V and of ΔL versus t for several values of a_o, for non-linear power profiles for several values of V_H

The information generated in steps (a) to (d) is universal for all Earth-Jupiter missions, within the range of a_o, V_H, and trip times used in the calculations. In other words, once this information is at hand, any Earth-Jupiter mission as defined in (a) can be analyzed. It is evident that the same kind of information can be generated for other general missions such as Earth-Mercury, close-solar, out-of-the-ecliptic, etc.

Having the universal plots of V and ΔL at hand, the mission analysis can proceed as follows:

1. note specified parameters such as α_{ps}, η versus I, etc.
2. define the mission profile, e.g. launch date, trip time, all forward thrust, thrust cut-off at arbitrary time t*
3. assume a value for I
4. assume a value for V_H
5. assign various values for a_o
6. calculate ΣL_i for each value of a_o
7. determine L from impulsive thrust information
8. determine the value of a_o where $L = \Sigma L_i$; this is the value of a_o that is required for the mission to be completed
9. calculate propulsion system mass and propellant mass for that value of a_o found in 8.
10. to find the optimum value of V_H, repeat 4. to 9. for several values of V_H
11. to find the optimum value of I, repeat 4. to 10. for several values of I
12. to find the optimum mission profile, observe the trends and alter the profile accordingly, e.g. vary t*

These calculations can be done quite simply by hand. Extensive variation of parameters might be done more easily with very simple computer programs. It appears that the general method could be adapted to the analog computer, which would provide very fast and very graphic means for approximate mission analysis.

CONCLUSIONS

Approximate mission analyses based on the Zola characteristic length have shown good agreement with precision digital-computer analyses for three different types of mission profiles. This good agreement increases confidence in the approximate methods, and serves as a rationale for further development of such methods.

It is concluded that these approximate methods:

a. could be used for preliminary screening of mission profiles;

b. could be used as an initial approximation in precision iterative digital-computer programs;

c. could be adapted for solution with analog computers.

REFERENCES

1. Zola, Charles L.: A Method of Approximating Propellant Requirements of Low-Thrust Trajectories. NASA TN D-3400. April, 1966.

2. Solar Powered Electric Propulsion Program. Program Summary Report, JPL Contract No. 951144. Hughes Aircraft Company SSD 60374R. December 1966.

3. Advanced Electric Propulsion Research. Semi-Annual Report for the period 1 January 1967 to 30 June 1967. NASA Grant NGR06-002-032. July, 1967.

4. Planetary Flight Handbook. Space Flight Handbooks, Volume 3, Part 2. NASA SP-35. 1963.

5. Planetary Flight Handbook. Space Flight Handbooks, Volume III, Part 5. NASA SP-35. 1966.

6. Layton, J. P.: unpublished analysis. Princeton University. 1967.

7. Sauer, Carl G.: Trajectory Analysis and Optimization of a Low-Thrust Solar-Electric Jupiter Flyby Mission. AIAA Paper No. 67-680. September, 1967.

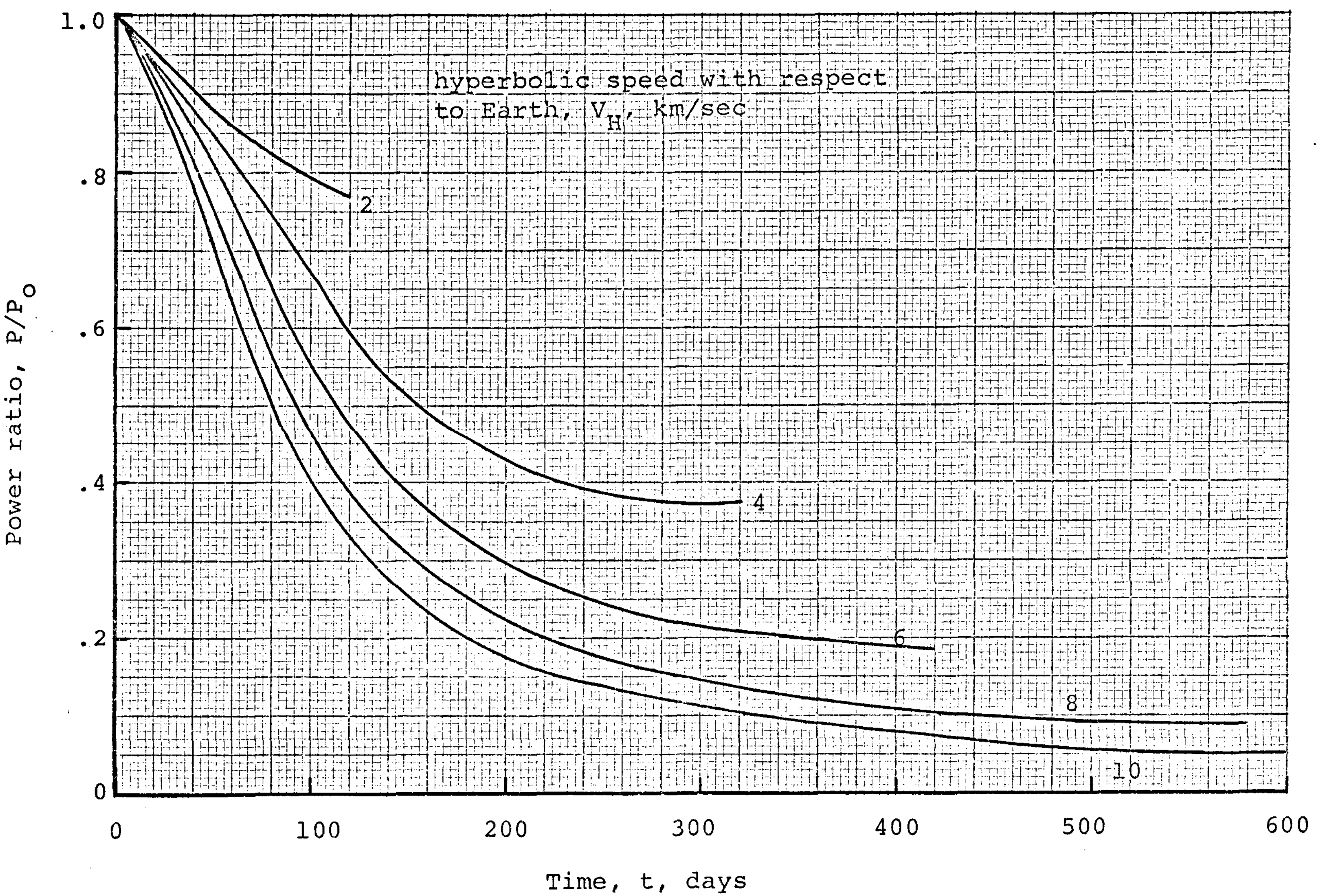

FIG. 1.1 Solar-array power profiles for impulsive-thrust trajectories outbound from Earth. V_H tangent to (mean) circular orbit of Earth.

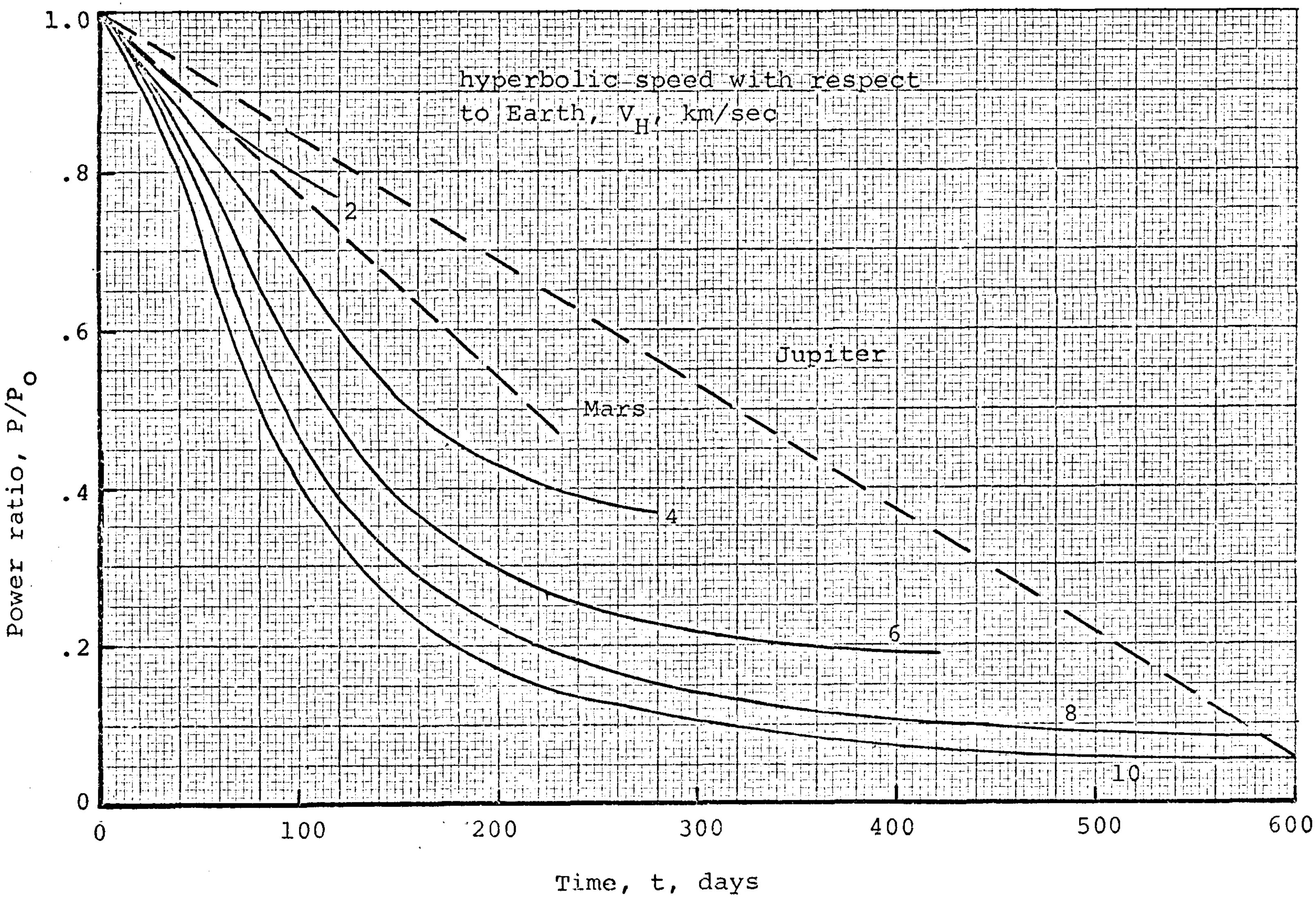

FIG. 1.2 Linear power profiles for 230-day Mars mission and for 600-day Jupiter mission. V_H tangent to (mean) circular orbit of Earth.

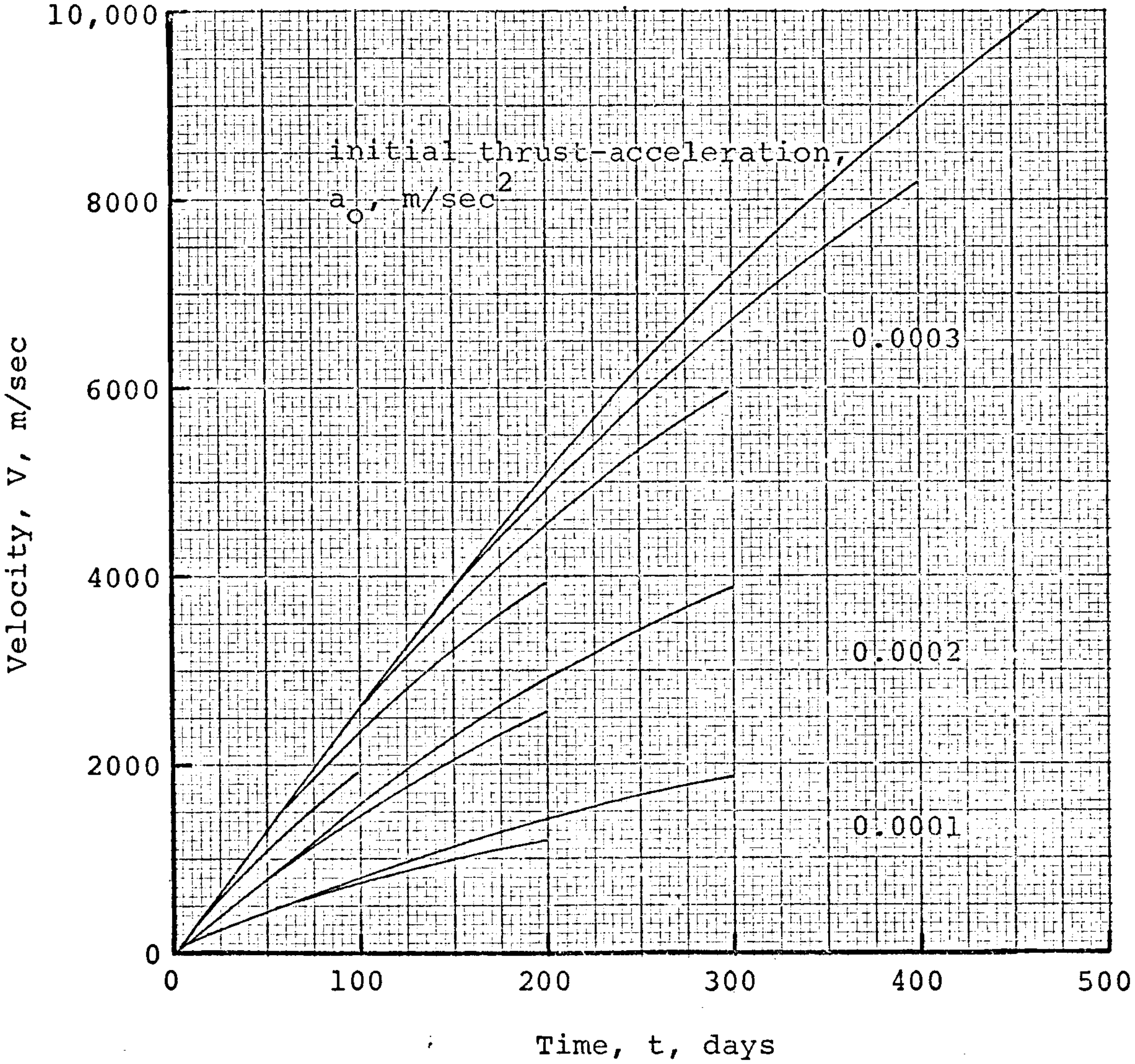

FIG. 1.3 Field-free, rectilinear velocity V for Earth-Mars heliocentric transfers with a linear power profile. Specific impulse, I = 4000 sec.

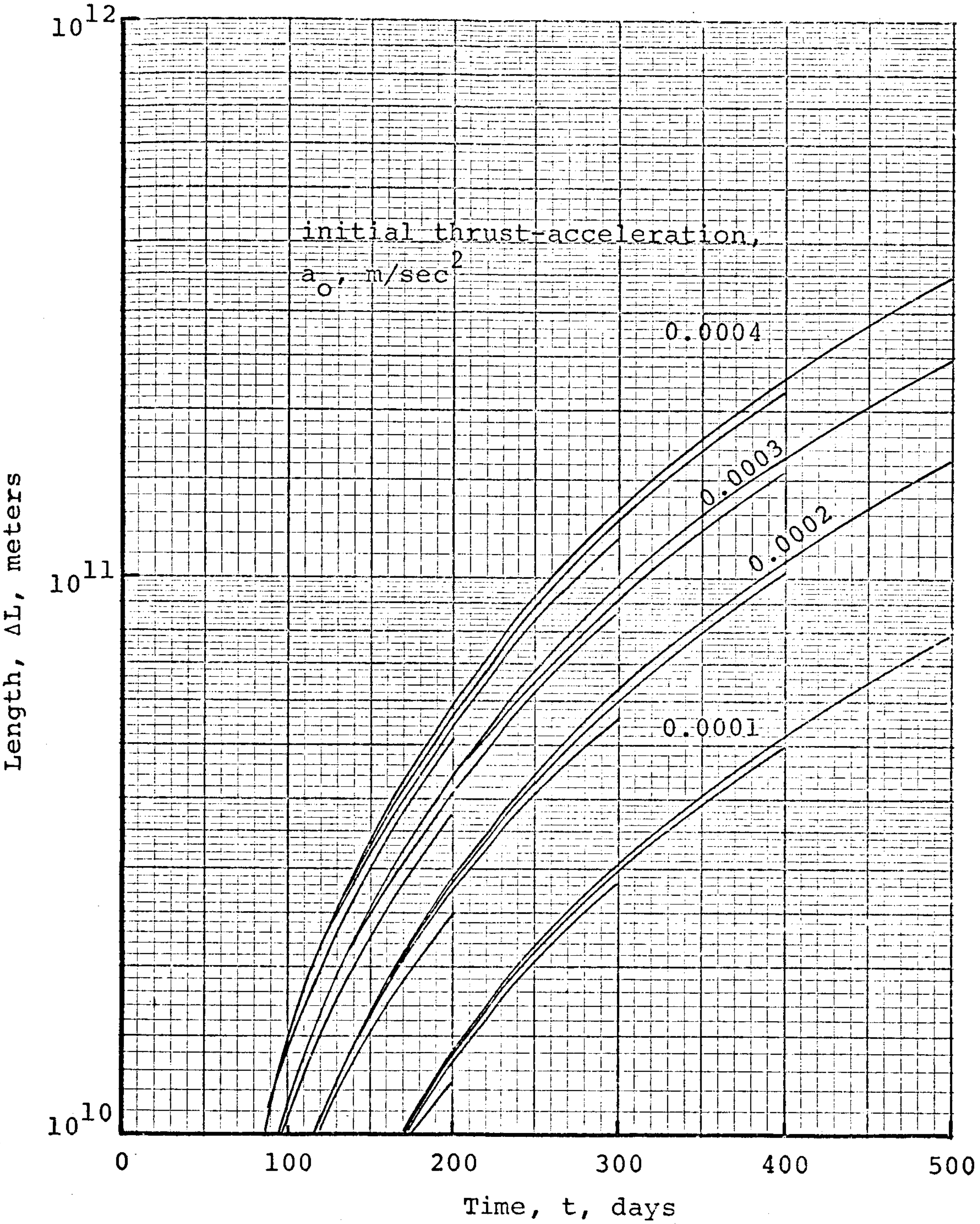

FIG. 1.4 Length ΔL for Earth-Mars heliocentric transfer with a linear power profile. Specific impulse, I = 4000 sec.

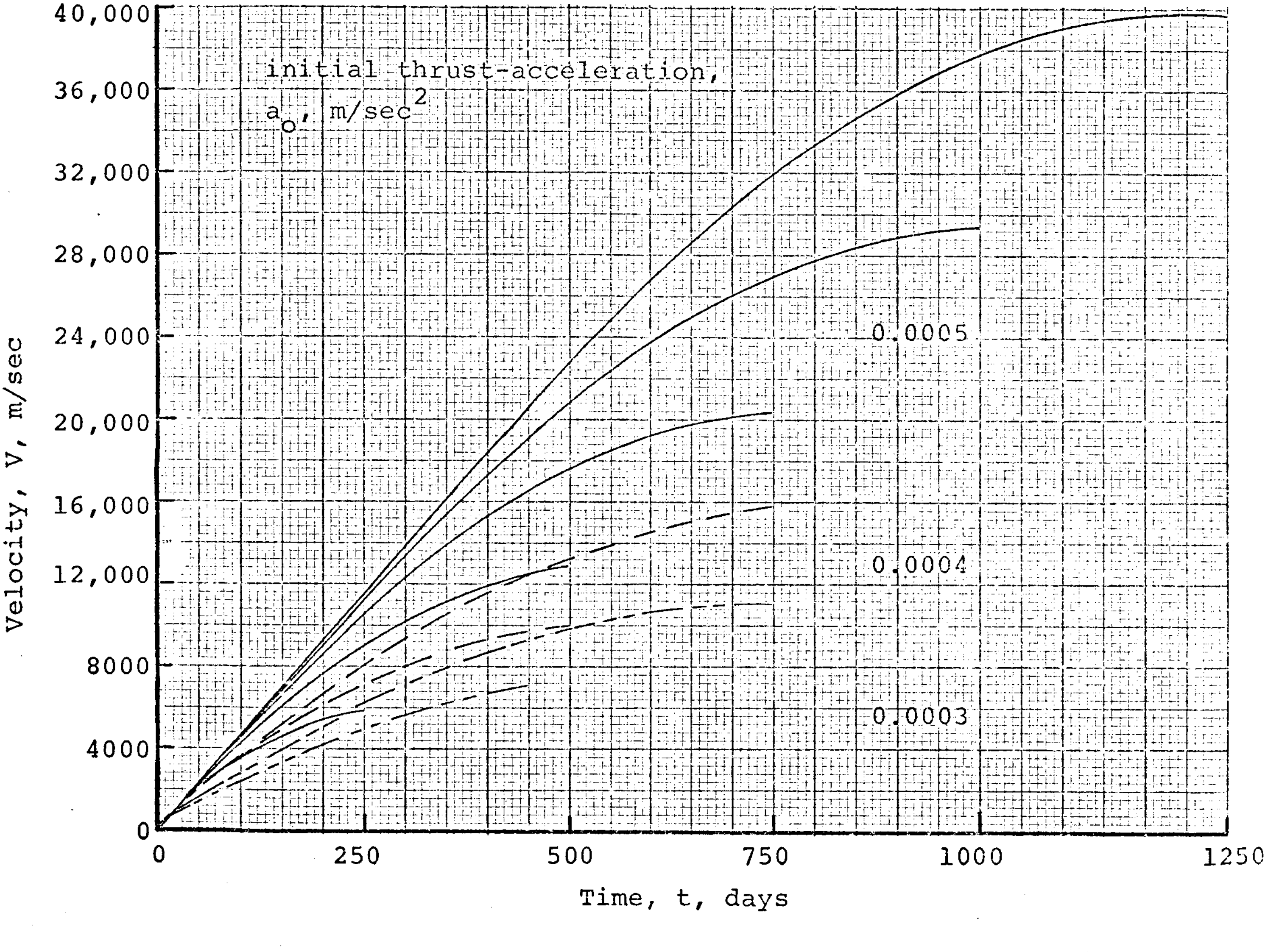

FIG. 1.5 Field-free rectilinear velocity V for Earth-Jupiter heliocentric transfers with a linear power profile. Specific impulse, I = 3500 sec.

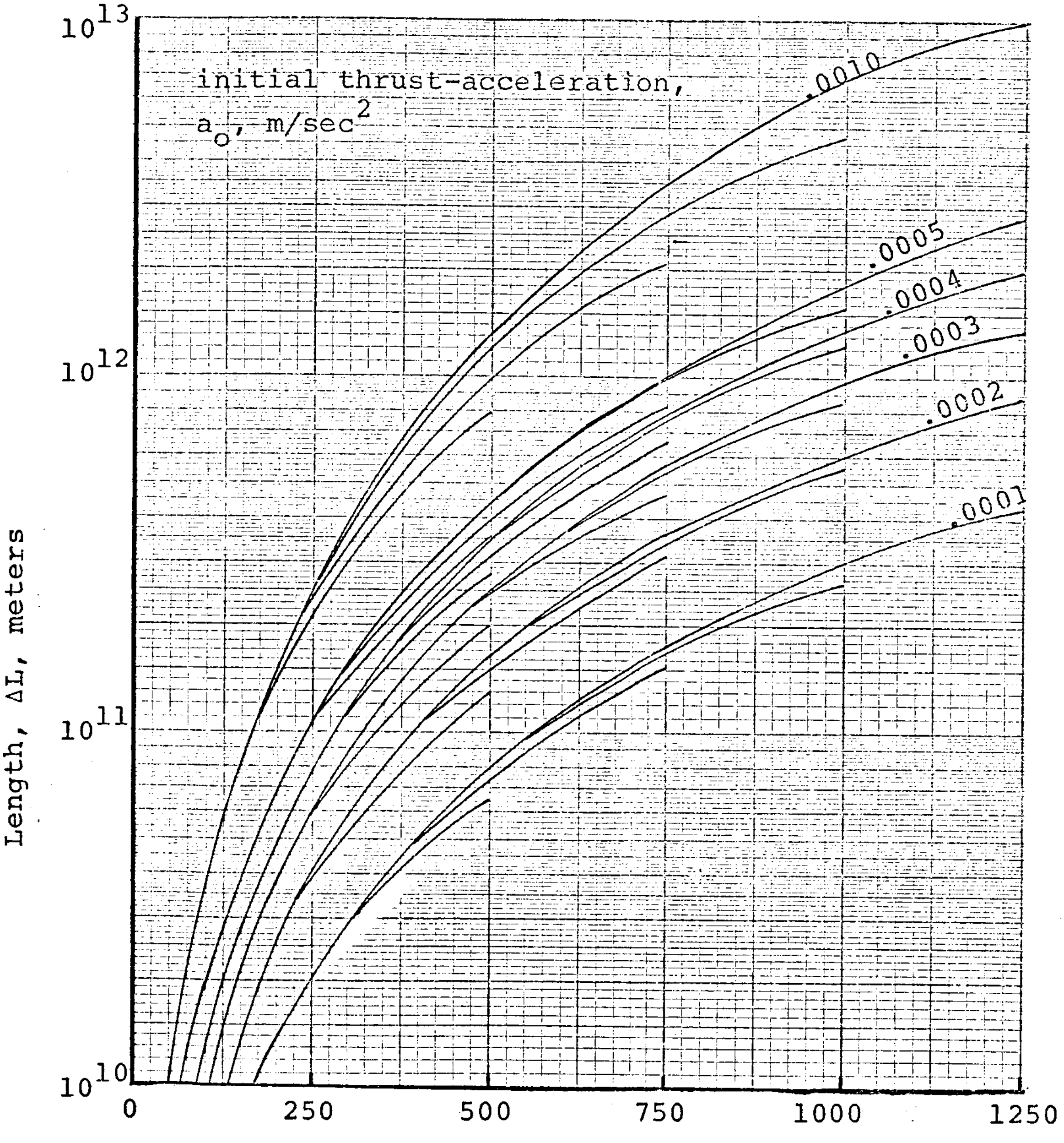

FIG. 1.6 Length ΔL for Earth-Jupiter heliocentric transfers with a linear power profile. Specific impulse, I = 3500 sec.

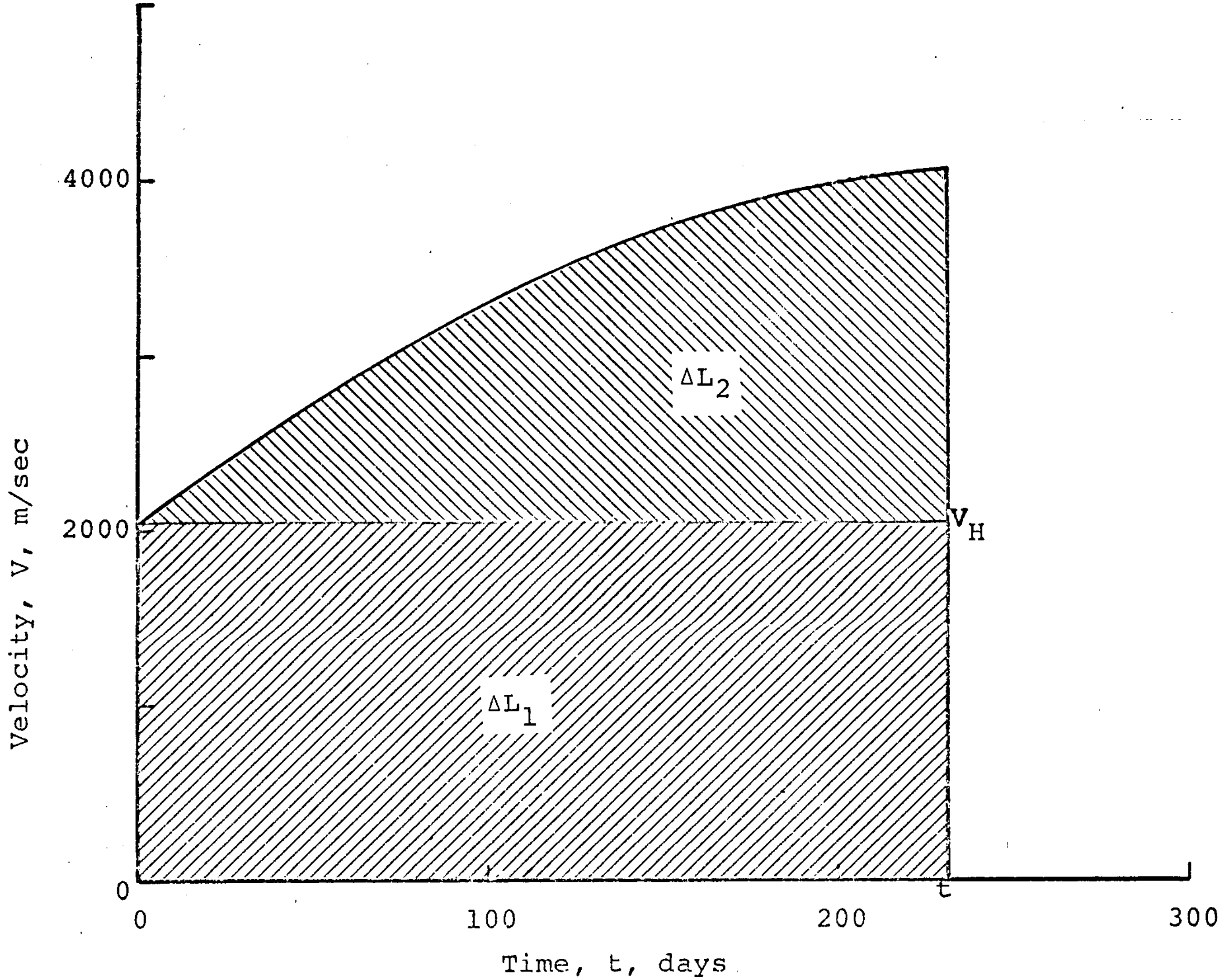

FIG. 1.7 Solar-electric 231-day Mars mission. $C_3 = 4.23\ km^2/sec^2$, $I = 4000$ sec.

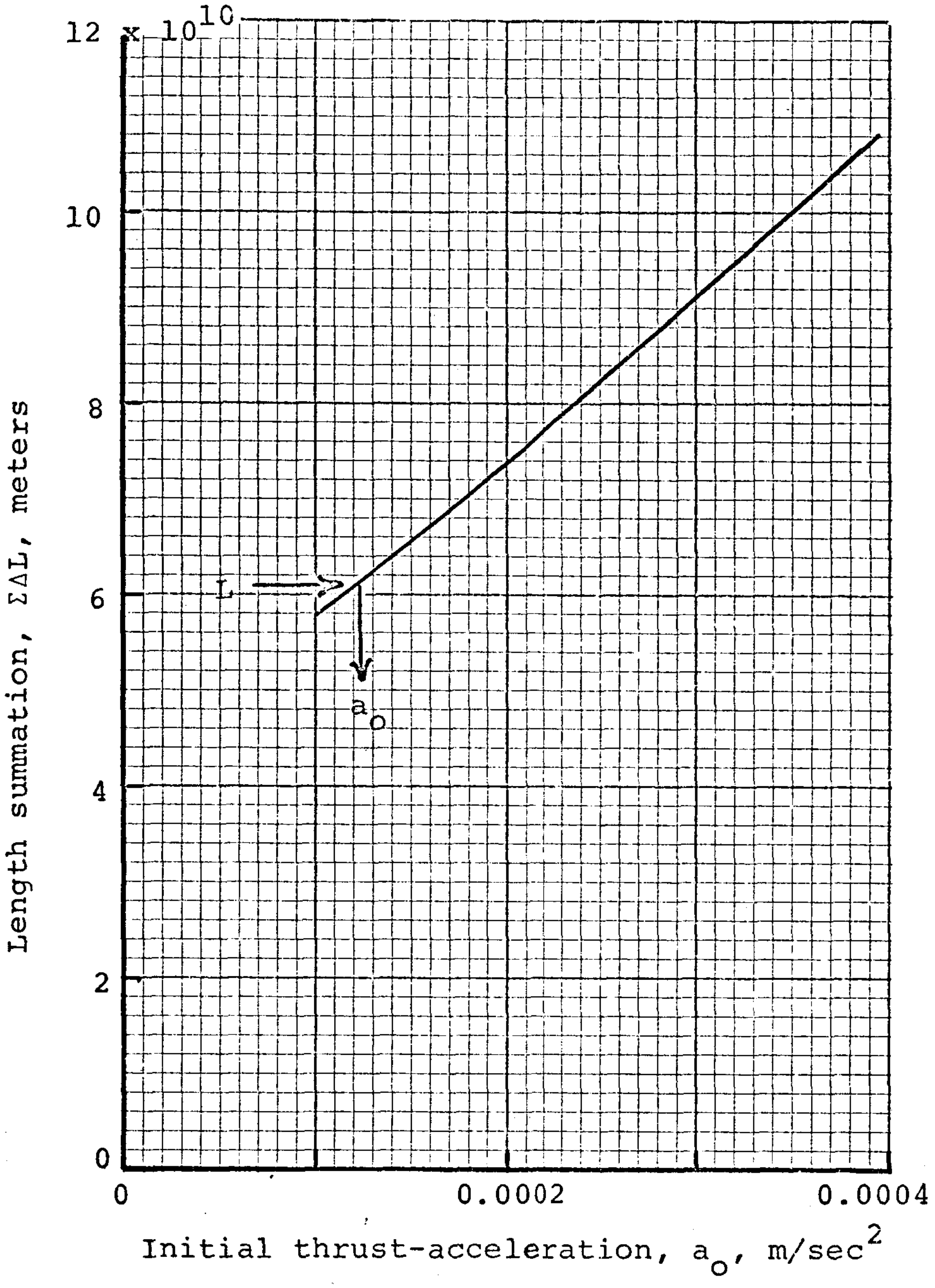

FIG. 1.8 Characteristic length as a function of initial thrust-acceleration for the 231-day Earth-Mars transfer with a linear power profile. V_H = 2.06 km/sec, and I = 4000 sec.

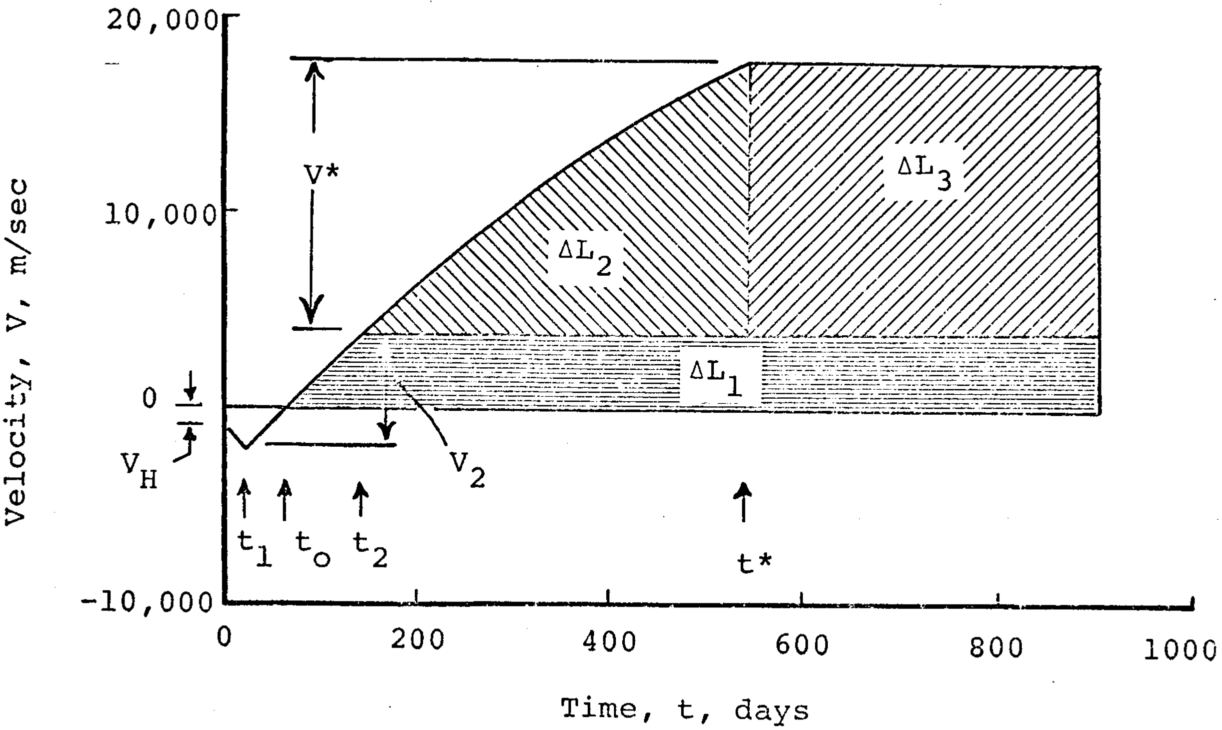

FIG. 1.9 Field-free rectilinear speed profile for 900-day Earth-Jupiter heliocentric transfer.

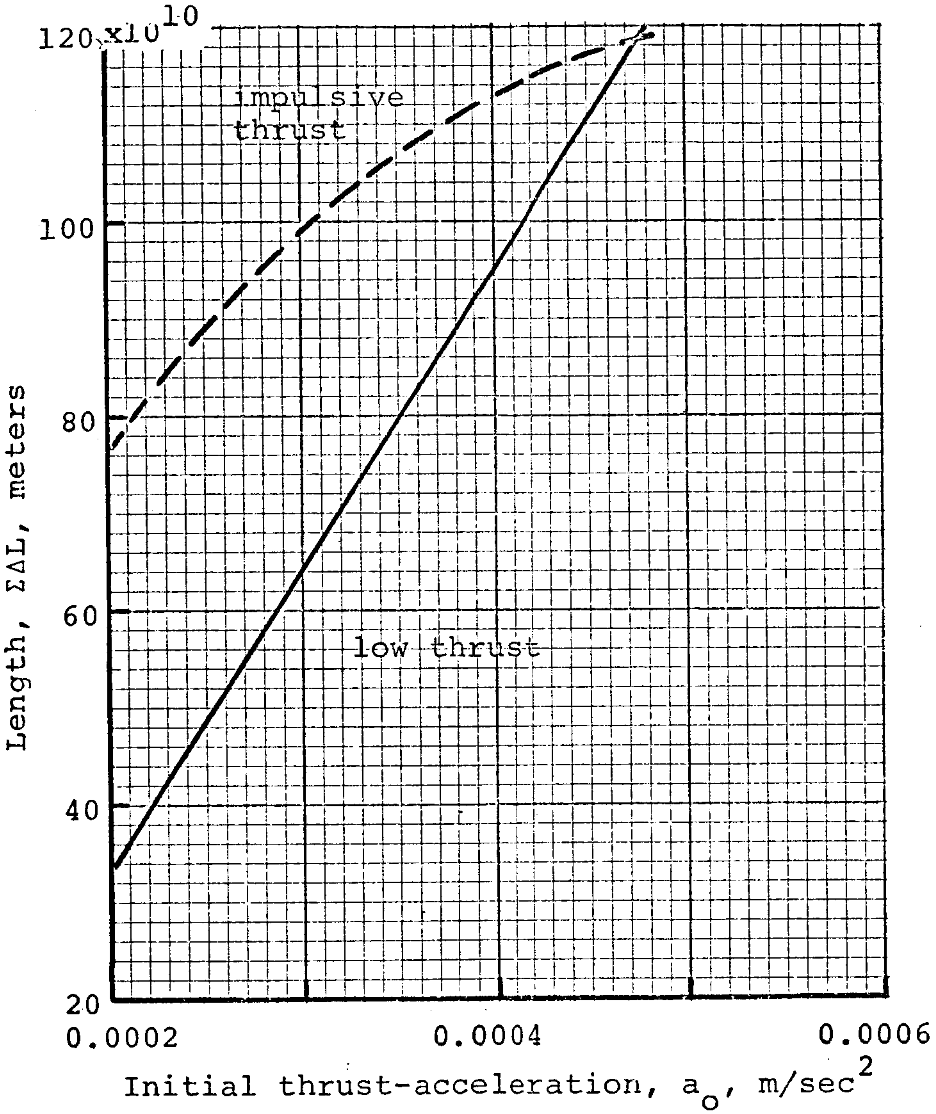

FIG. 1.10 Characteristic length as a function of initial thrust-acceleration for the 900-day Earth-Jupiter transfer with a linear power profile. V_H = 1.1 km/sec (reverse), and I = 3500 sec.

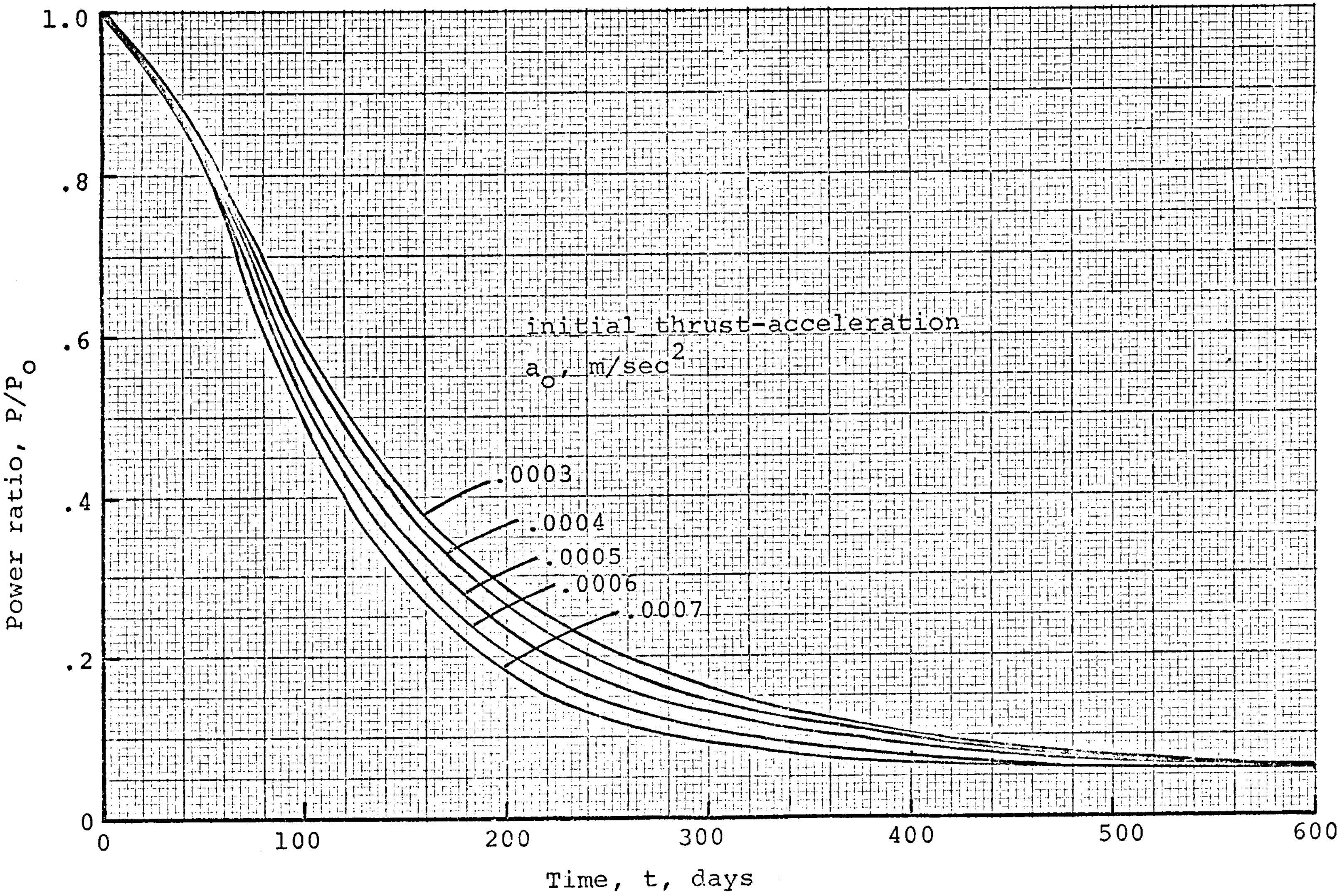

FIG. 1.11 Power profiles for 600-day Earth-Jupiter heliocentric transfer, estimated with the characteristic length method. V_H = 4 km/sec, I = 3,230 sec.

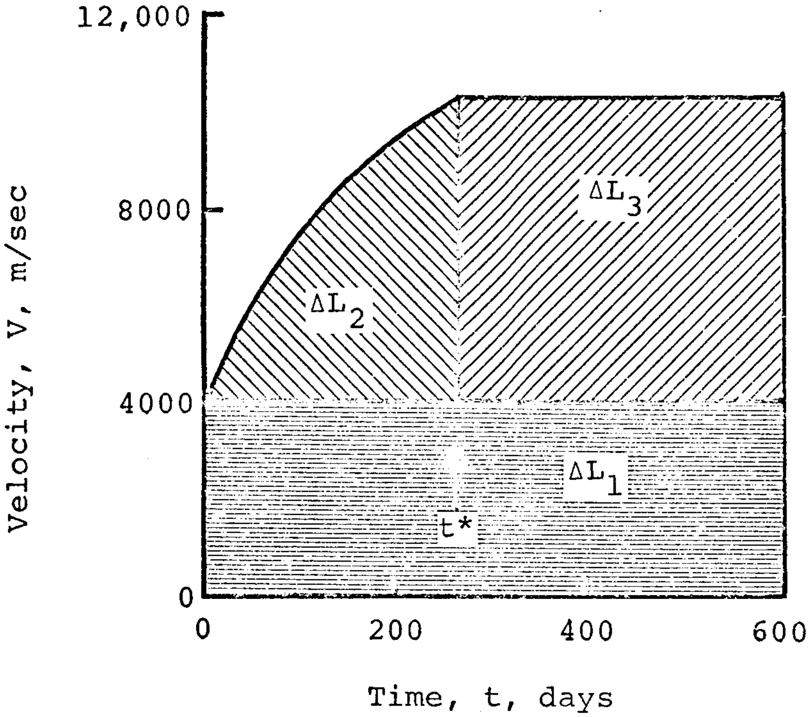

FIG. 1.12 Field-free rectilinear speed profile for 600-day Earth-Jupiter heliocentric transfer. $V_H = 4$ km/sec.

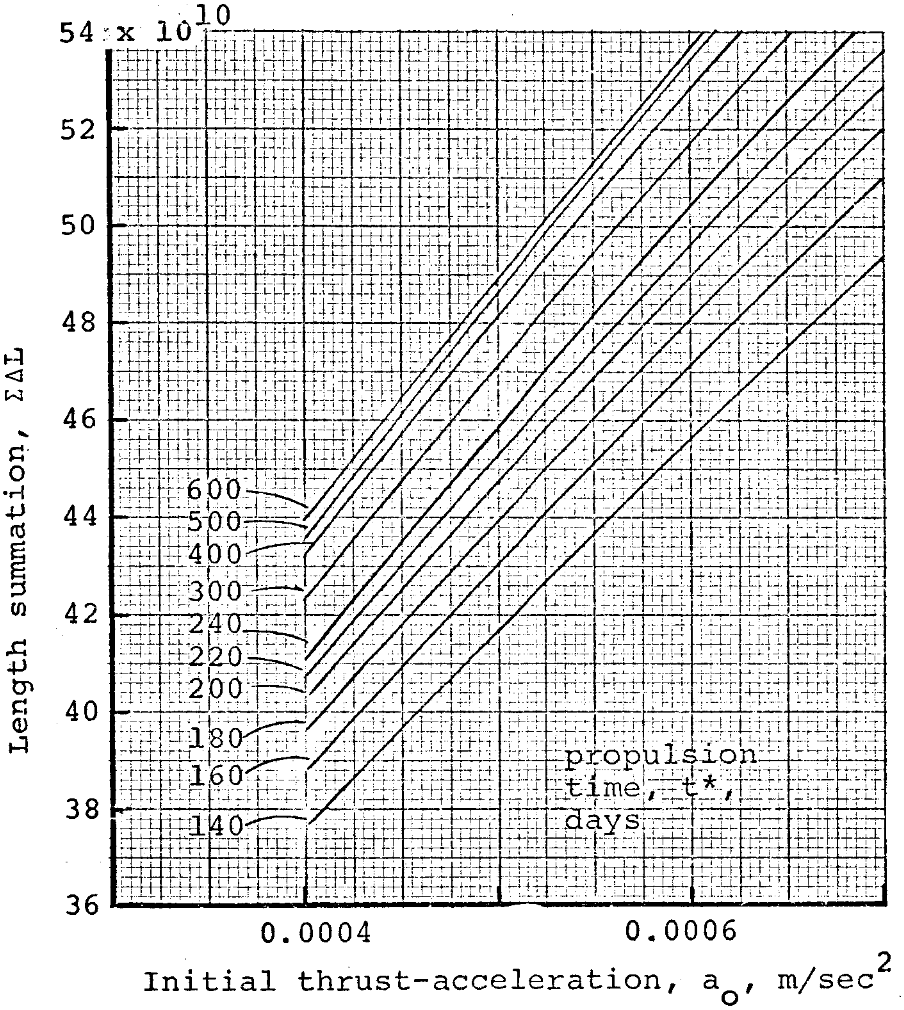

FIG. 1.13 Characteristic length as a function of initial thrust-acceleration and of propulsion time for the 600-day Earth-Jupiter transfer with a non-linear power profile. V_H = 4 km/sec, and I = 3230 sec.

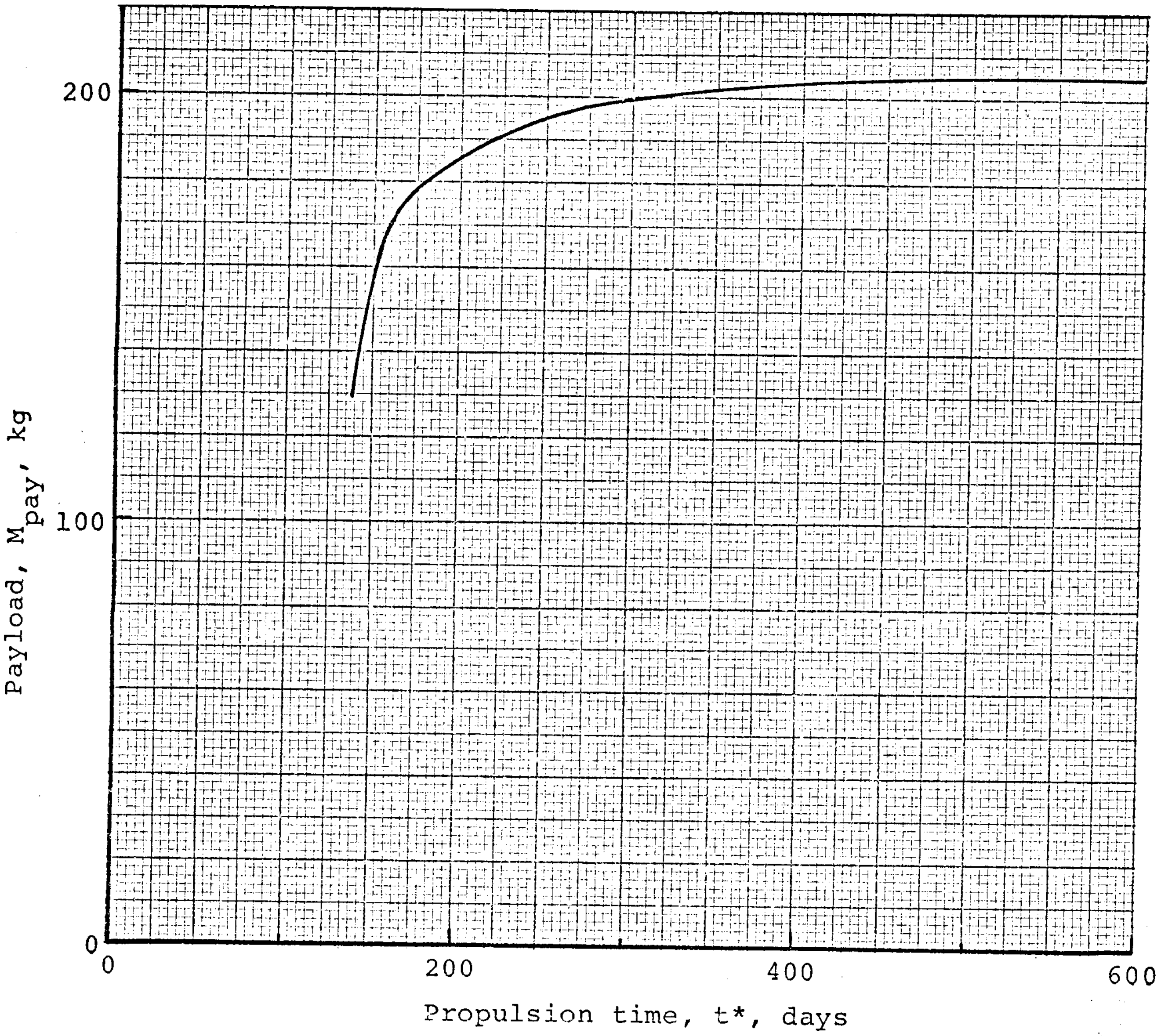

FIG. 1.14 Payloads for 600-day Jupiter fly-by. V_H = 4 km/sec, I = 3230, α_{ps} = 30 kg/kwe, k = 0.1.

GENERAL RELATIVITY AND SPACE PROPULSION

S. Basri, W. R. Mickelsen, and
R. T. Hodgson

The theory of general relativity has been reviewed for possible applications to space propulsion. Because of the brief time available for this review, no investigation was made of the consequences of changing any of the basic postulates of the theory. That is, the theory of general relativity was assumed to be valid and complete.

Three possible applications to space propulsion were found, and these are described here. These possible applications have received only a cursory examination; further, there may well be other possible applications not discovered in the present brief review.

Negative Mass

The consequences of the possible existence of negative mass were investigated because such mass could be used to accelerate ordinary mass. Bondi[1] has pointed out that a pair of equal and opposite active gravitational masses will accelerate uniformly and without limit if the action is confined to the line of centers. This would be of obvious importance for space vehicle applications.

A distinction may be made between three types of masses according to the measurement by which they are defined: inertial mass is defined as the constant that enters Newton's second law ($F = ma$). Passive gravitational mass is that mass upon which a gravitational field acts, and active gravitational mass is that mass which acts as a source of gravitational fields. In more fundamental terms[2], inertial mass is that property of matter which resists changes in motion, passive gravitational mass is that property of matter which responds to a gravitational field, and active gravitational mass is that property of matter which induces a gravitational field.

According to the principle of equivalence which is one of the fundamental postulates of general relativity, the passive gravitational mass is equal to the inertial mass. However, there is nothing in the general theory of relativity to relate the active gravitational mass to the passive or inertial masses. Within this theoretical framework, the consequences of negative and positive active gravitational mass can be examined.

Consider a body of active gravitational mass $M_{A.G.}$ acting on another body with passive gravitational mass $m_{P.G.}$ and inertial mass m_I.

The inertial mass enters into the law of motion:

$$\vec{F} = m_I \, \vec{a}. \tag{1}$$

For a coordinate system fixed in the center of mass $M_{A.G.}$ and with the weak field approximation, equation (1) becomes:

$$\vec{F} = m_I \vec{a} = - \frac{G \, M_{A.G.} \, m_{P.G}}{r^2} \, \vec{e}_r \tag{2}$$

where G is a number which is assumed to be the same for all active gravitational masses, r is the distance between the center of masses $m_{P.G.}$ and $M_{A.G.}$, and $\vec{e}_r$ is a unit vector in the radial direction.

According to the principle of equivalence:

$$m_{P.G.} = m_I \tag{3}$$

and hence:

$$\vec{a} = - G \, \frac{M_{A.G.}}{r^2} \, \vec{e}_r \tag{4}$$

It is clear from equation (4) that the acceleration of a body towards or away from $M_{A.G.}$ is independent of any sign of mass of the body and depends only on the sign of $M_{A.G.}$ A body with positive active gravitational mass will cause all bodies to fall toward it with equal accelerations, while one of negative active gravitational mass will repel all bodies. The case of positive and negative mass is not analogous to the "like charges repel, unlike charges attract" electrostatic case.

If a body A with a positive active gravitational mass is in the neighborhood of a body B with the same absolute value of a negative active gravitational mass, then body B will accelerate towards body A under the influence of A's gravitational field. At the same time, body A will be acted upon by body B's gravitational field and accelerate away from B. The two bodies will have the same direction and magnitude of acceleration; their position relative to one another will not change, and they will accelerate uniformly without limit.

The magnitude of such acceleration can be easily calculated for bodies of different shapes. Consider two spheres of radius R and mass $M_{A.G.}$ a distance r from one another. The acceleration can be calculated from equation (4):

$$a = \frac{G\, M_{A.G.}}{r^2} \qquad (5)$$

The acceleration may be compared to the acceleration of gravity at the Earth's surface:

$$\frac{a}{g} = \frac{M_{A.G.}}{r^2}\,\frac{R_E^{\,2}}{M_E} = \frac{1}{4}\,\frac{\rho_{A.G.}}{\rho_E}\,\frac{R}{R_E} \qquad (6)$$

where M_E and R_E are the mass and radius of the Earth, and ρ is density. If the density of the bodies is assumed to be Earth density, and r is taken to be 2R, equation (6) reduces to:

$$\frac{a}{g} = \frac{1}{4}\,\frac{R}{R_E} \qquad (7)$$

For an acceleration of 10^{-4}g, the bodies (of Earth density, 5.5 gm/cc) would have diameters of about 2.5 miles, and for an acceleration of 10^{-5}g the diameters would be about 1/4 mile. Osmium has a density of 22.5 gm/cc, so bodies of osmium would have diameters of about 300 feet for an acceleration of 10^{-5}g. Density of matter in neutron stars may be of the order of 10^{15} gm/cc, so if super-density matter was available, the two bodies could be quite small.

If the two bodies were in the form of parallel disks of thickness t, and radius R, and separated by a distance d, the acceleration is given by the equation:

$$\frac{a}{g} = \frac{3}{2}\, t/R_E \,, \tag{8}$$

where $t << d << R$ and the mass density of the disks is equal to the mean earth density. Equation (8) follows from Gauss' law in complete analogy with electrostatics. From comparison of equations (7) and (8), it appears that a reduction in body dimension by a factor of six could be achieved with a flat-disc configuration.

It is difficult to deny the existence of negative mass on strictly experimental grounds. For instance, a body with negative active gravitational mass and positive inertial mass could only be detected by the effects of its own gravitational field on another body. It would be attracted to the Earth's surface (have weight) and be accelerated in the conventional Newtonian direction by any force. The only means of detection of such a body would be a Cavendish Balance measurement of gravitational forces between masses. Inconsistencies of one part in 10^5 could be noted.

Any body with negative inertial mass would behave very oddly. A force applied to the body would cause it to move in the opposite direction to the force. However, such a body of macroscopic size would hardly be found on the Earth's surface (or Moon, or asternoid). It would try to reach the center of the Earth under the influence of the Earth's gravitational field. The stresses that would be set up in the body if it were resting on the Earth's surface would grow without limit since the reaction force "outward" would push the body "inward". Such negative inertial mass would break up and tend to find an equilibrium position in the center of the Earth. If the active gravitational mass of such negative inertial mass were also negative and concentrated in a sphere of radius R_N about the origin, the Earth's gravitational field, $\underline{a}$, would have the radial dependence shown in Fig. 1b instead of the customary dependence shown in Fig. 1a. This is the same gravitational potential that would arise from a hollow sphere depicted in Fig. 1c.

The geometries depicted in Fig. 1 show that the moment of inertia of the Earth would be increased. If R_N/R_E is sufficiently large, it may be possible to detect such a mass distribution by measuring the gravitational acceleration as a function of distance below Earth's surface because the slope is affected by the value of R_N/R_E.

Bondi[1] has constructed a metric for the case of two equal but opposite sign active gravitational masses in uniform acceleration discussed earlier. He concludes that, if the active gravitational mass is negative, the inertial mass must also be negative. This can be shown on physical grounds. If the inertial masses of the two bodies were both positive, the energy of the system ($E = m_I\, c^2$) increases without limit and energy is not conserved. For one positive inertial mass and one negative inertial mass, the total inertial mass is zero and the energy of the system remains zero. If the conservation of energy principle is accepted, a body with negative active gravitational mass must have negative inertial mass.

Non-Newtonian Forces

An equation for the motion of a mass in the field of a much larger mass M was derived by Weber[3]. According to this equation, if $\vec{v}$ and $\vec{a}$ are the velocity and acceleration of M, respectively, and $\vec{R}$ is the position vector from m to M, then in the limit of weak fields and $(v/c)^2 \simeq 0$, the force $\vec{F}$ exerted by M on m is given by:

$$\frac{\vec{F}}{m} = \frac{GM}{R^2}\,\vec{e}_R + \frac{4GM}{c^2 R}\,\vec{a} + \frac{4GM}{c^3}\,\frac{\vec{a}.\vec{R}}{R^2}\,\vec{v} \qquad (9)$$

The first term is just the usual gravitational attraction between two masses, but the other two terms are strange to Newtonian mechanics, and show that two additional forces are exerted on m, which are proportional to $\vec{v}$ and $\vec{a}$. In order to get a feeling for the relative influence of these forces, a calculation is made here of the acceleration of a rocket near the surface of the earth due to the orbital speed v = 30 km/sec of the earth, and its centripetal acceleration $a = 0.6$ m/sec^2 due to rotation around the sun. The second term is 1.7×10^{-8}g and the third term is 1.7×10^{-10}g, where $g = GM_E/R_E{}^2 = 9.8$ m/sec^2.

However, in the neighborhood of a binary neutron star, the space ship could gain an acceleration in excess of 10^6g, as was pointed out by Forward[4]. Such accelerations could be used to give the space ship speeds near the speed of light.

Other applications of these forces to space travel are discussed by Dyson[5] in his article "Gravitational Machines".

Distortion of the Metric

Since the metric determines the geodesic which a space vehicle follows, it might be possible to accelerate the vehicle by distortion of the metric in its neighborhood. For example, if the distortion of the metric just enclosed the volume of the vehicle, then a distortion of the order of one cubic meter would be required to accelerate the vehicle. The power required to maintain the distortion of the metric would be roughly equal to rate of energy consumption needed to continuously distort the metric just forward of the vehicle, assuming that the energy used to distort the metric could not be regained after passage of the vehicle.

The energy required to distort the metric can be estimated by determining the energy density u of a gravitational field that produces an acceleration of about 10^{-4}g. Comparing the expressions for energy densities of electric and gravitational field from point sources:

$$E_Q = \frac{F_Q}{q} = \frac{Q}{4\pi\varepsilon_o r^2} \qquad (10)$$

$$E_M = \frac{F_M}{m} = \frac{GM}{r^2} \qquad (11)$$

it is evident that $4\pi\varepsilon_o$ corresponds to 1/G. The electric field energy density is $\varepsilon_o E_Q^2/2$, so the gravitational field density is:

$$u = \frac{E_M{}^2}{8\pi G} \qquad (12)$$

where $E_M = F_M/m = ma/m = a$ is the acceleration. For $a = 10^{-4}$g, the gravitational field density is u = 600 joule/m^3.

If the gravitational field is generated by a spherical mass distribution M of radius R, then acceleration at the surface is:

$$a = GM/R^2 \tag{13}$$

For $a = 10^{-4}g$:

$$GM/R^2 = 10^{-4}GM_E/R_E{}^2 \tag{14}$$

where the subscript E refers to Earth. For a mass density equal to that of Earth:

$$R = 10^{-4}\ R_E = 0.4 \text{ mile} \tag{15}$$

which corresponds to a mass of 6×10^{12}kg. The reason for such a high mass is that the gravitational field extends over all space, so much of it is wasted.

Another possible way of distorting the metric is by a pulse of gravitational radiation. But such radiation travels at the speed of light, and hence cannot be utilized.

Radiation of gravitational waves in the backward direction can also accelerate a rocket. This does not seem practical, however, since the effect is too weak and the efficiency of generating such radiation is low.

Although there is no known practical way of distorting the metric, it is of interest to calculate power requirements for an imagined means of metric distortion.

If the vehicle is assumed to begin its journey moving at Earth's orbital velocity, then the initial velocity is about 30 km/sec. The power required would be the product of velocity and energy density; so for a one square meter frontal area of the vehicle, and for an acceleration of 10^{-4}g, the power required would be $30 \times 10^3 \times 600 = 18 \times 10^6$ joule/sec, which is 18 megawatts. For an acceleration of 10^{-5}g, the power requirement would be 180 kilowatts. Space power generation systems presently envisioned with power levels of the order of 100 kilowatts have physical dimensions much larger than one cubic meter. However, a high-density mass might be mechanically connected to the ship and the distortion of the metric need be of a size only large enough to envelop the high-density mass. In this way, the power requirement could be appreciably reduced.

REFERENCES

2.1. Bondi, H., Revs. Mod. Phys. 29, 423 (1957).

2.2. Jammer, M.: *Concepts of Mass*. Harvard University Press. (1961).

2.3. Weber, J.: *General Relativity and Gravitational Waves*, Interscience Publishers, New York (1961).

2.4. Forward, R., Am. J. Phys. 31, 168 (1963).

2.5. Dyson, F.: *Interstellar Communication*, A. Cameron, Editor, W. A. Benjamin, New York (1963).

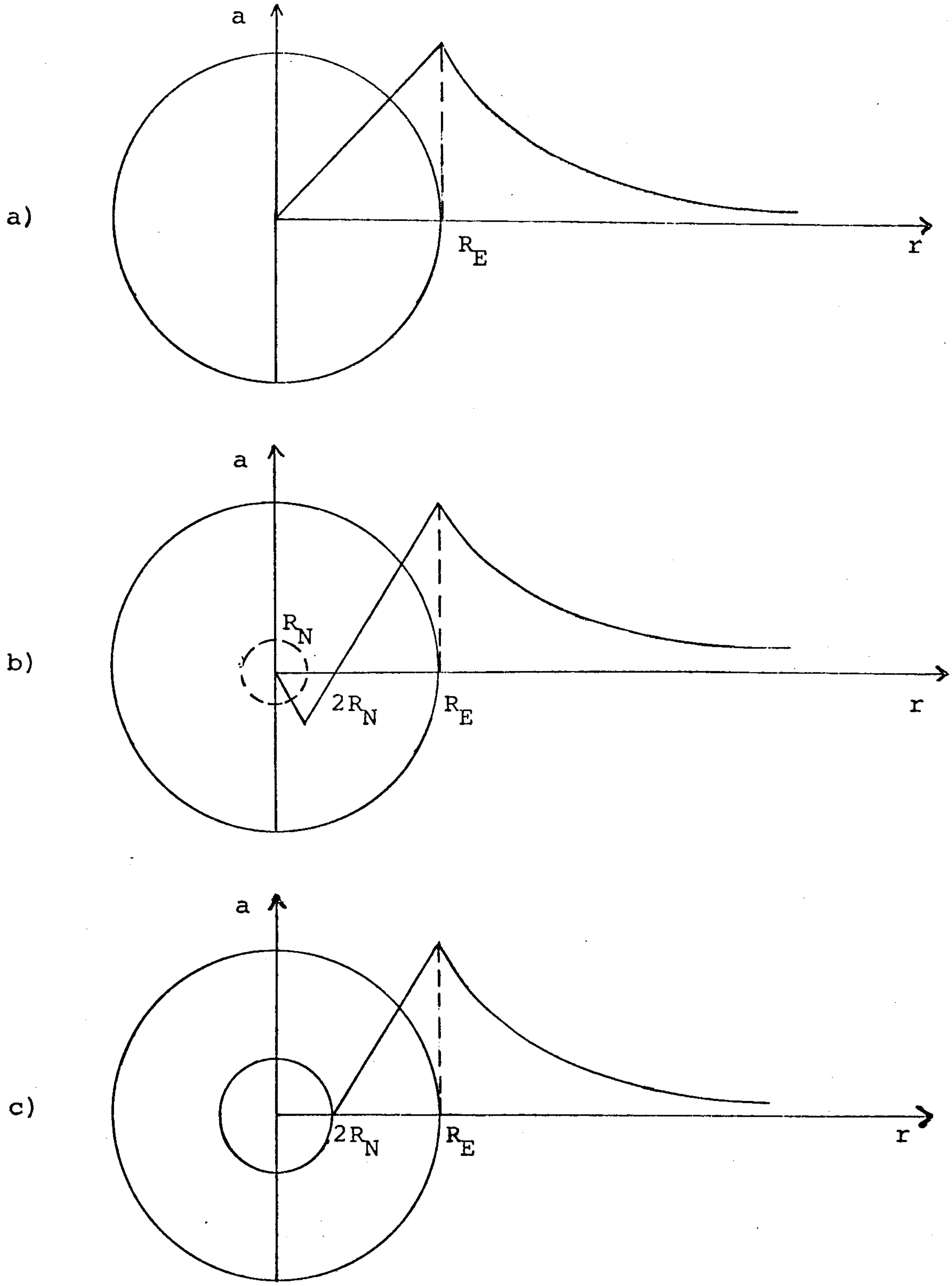

FIG. 2.1. - Acceleration of Gravity as a Function of Radius for Three Mass Distributions a) Solid Positive Mass Distribution b) Negative Active Gravitational Mass at Earth's Center c) "Hollow" Earth Resulting from Mass Distribution Depicted in "b"

POWER LOSS IN MERCURY-AND CESIUM-BOMBARDMENT THRUSTERS

by W. R. Mickelsen

Electron-bombardment thrusters have been developed for both mercury[1,2,3] and cesium[1,4,5] propellants. Performance of these thrusters has been comparable, but much research and development remains before ultimate performance can be attained. For example, present performance of the mercury-bombardment thruster includes a discharge power loss of over 200 ev/ion, which is much greater than the theoretically possible discharge power loss of 10.4 ev/ion (ie, the first ionization potential). That great improvements are possible is shown by the 50 ev/ion obtained some time ago with cesium hollow-cathode discharges[6].

Because of the great disparity between the present-day discharge energy loss and the first ionization potential, it is of interest to examine the various loss mechanisms more deeply. From such examinations may come a better estimate of the practical lower limits of discharge losses in mercury-and cesium-bombardment thrusters.

Discharge Currents and Power Loss

Ionization of neutral-atom propellant is achieved in electron-bombardment thrusters by electron impact. Electrons emitted from a cathode are quickly accelerated by falling through a sheath potential difference of about 30 volts for mercury and about 8 volts for cesium. There is a radial electric field reaching out to the enclosing cylindrical anode, and an imposed axial magnetic field, so the electrons follow cycloidal paths about the axis of the chamber. Electron energies become randomized[7], presumably by plasma instabilities. After collisions and diffusion by mechanisms such as plasma turbulence[8], the primary and secondary electrons arrive at the anode. Because of the randomization of electron energy, some electrons may reach the screen grid and walls even if these surfaces are maintained at cathode potential.

Ions generated in the discharge may suffer three fates:

a. fall from the plasma to the screen grid and wall, and recombine there to be injected again into the discharge as neutral atoms

b. fall from the plasma to the anode, recombine and re-enter the discharge as neutral atoms

c. be extracted from the plasma into the accelerator system.

Recombination in the plasma proper is negligible at the particle densities commonly used in bombardment thrusters.

The electron and ion currents are shown in Figure 3.1. Ion fates are J_b^+ ion current to the accelerator, J_a^+ recombined on the anode, and J_w^+ recombined on the wall, and the total ion generation in the plasma is represented by the current J^+. Electron current from the anode is J_A^-, and is made up of some of the primary electron current J_d^- (from the cathode), most of the secondary electron current J_i^- (electrons from the ionization of neutral atoms), and the electrons needed to recombine with the ions striking the anode represented by J_{ar}^-. Cathode current J_d^- is roughly made up of the current J^+ of electrons that are successful in causing ionization, of the unsuccessful electrons that diffuse to the anode without causing ionization, and of electrons that are lost to the wall and the screen grid.

From this cursory description of ion and electron currents, it should be evident that current measurements with ammeters cannot provide magnitudes of ion and electron currents, particularly at circuit junctions such as the wall and screen grid. Only rough trends can be deduced from ammeter readings, such as that the ratio of anode current to ion beam current, J_A^-/J_b^+ is about 10 for contemporary thrusters.

In general, the total power consumed in the discharge is the net anode current $(J_A^- - J_b^+)$ times the potential difference between cathode and anode. Somewhat different definitions of discharge power may be used in practice, depending on the details of the circuitry.

Fundamental Loss Mechanisms

There appear to be three mechanisms in which electric power is consumed but not converted to thrust in bombardment thruster ionization chambers:

a. loss of ions by recombination at the walls, screen grid, anode, and cathode surfaces
b. loss of energetic electrons by diffusion or by plasma instabilities resulting in energy randomization, before the electron can contribute to the ionization process
c. loss of electron energy by collisions

The first two of these loss mechanisms are highly dependent on physical geometry and on the field configuration in the ionization chamber. The third loss mechanism appears to be amenable to direct analysis, as described in the following section.

Power Loss in Ion Generation

There are many kinds of collisions by which electrons may lose energy in the discharge. Of these, the most important appear to be collisions with neutral propellant atoms in which the atom energy is raised to an excited state, or to an ionized state. Although detailed calculations have not been attempted, the semiclassical method of Gryzinski[9,10] has provided the basis for an approximate analysis[11] that is applicable in principle to any atomic propellant. In this approximate analysis, the following assumptions are made:

a. excitation and ionization cross sections are represented by the Gryzinski expressions
b. electrons lose energy by excitation collisions in the energy range from the first excitation potential to the first ionization potential
c. electrons lose energy by ionizing collisions in the energy range above the first ionization potential (only the singly-ionized state is accounted for)

d. elastic collisions are negligible, since $\Delta E/E \doteq 2m_e/m_o \leqslant 5 \times 10^{-4}$
e. metastable states are neglected
f. wall recombination losses are not accounted for
g. electron diffusion losses are not accounted for
h. cumulative inelastic collisions are improbable (because collision frequencies for excited states are much less than the radiative transition frequencies).

The approximate analysis for the general atom has been done for two cases: a mono-energetic beam of electrons interacting with neutral atoms, and a Maxwellian swarm of electrons interacting with neutral atoms. In the work being reported here it was assumed that:

i. electrons entering the discharge become randomized immediately to a Maxwellian energy distribution.

With the assumptions listed above, the approximate theory[11] for the general atom can be summarized as shown in Figure 3.2 where the normalized ion-generation energy loss is plotted against the ratio of first-excitation to first-ionization potentials, with the ratio of electron kinetic temperature to first-ionization potential as the parameter. The information presented in Figure 3.2 can be used to estimate ion-generation energy loss for any atomic propellant when the excitation and ionization potentials are known.

Excitation and Ionization Cross Sections

Excitation cross sections for mercury[12-17] are shown in Figure 3.3. These cross sections were deduced from the data in the literature, and are summed in Figure 3.4. From inspection of Figure 3.4 it is evident that excitation levels are as low as 2 ev for mercury, which is considerably lower than values previously quoted in the electric propulsion literature[7,18]. Excitation cross sections[12,13,19-25] for cesium are summarized in Figure 3.5.

Fundamental Energy Loss in Ion Generation

From the preceding data on excitation and ionization cross sections, the lower excitation potentials ϕ_ℓ and first ionization potentials ϕ_i for mercury and cesium are:

	mercury	cesium
ϕ_ℓ, ev	~3	~1.4
ϕ_i, ev	10.4	3.89
ϕ_ℓ/ϕ_i	~0.3	~0.36

By inspection of Figure 3.2, it is clear that mercury and cesium will have roughly the same values of (ev/ion)/ϕ_i in the electron temperature range of interest which is[7] $kT_e = 1$ to 10 ev. This amounts to the conclusion that ev/ion in mercury and cesium bombardment thrusters will be roughly proportional to the first ionization potentials of these two propellants. In other words, mercury bombardment thrusters will always have about 2.5 times the discharge power loss of mercury bombardment thrusters.

The validity of this conclusion depends on several important factors. If the primary loss mechanism is the diffusion of electrons to the walls, anode, and screen grid, then the fundamental ion generation energy loss calculated above will not be important. But if the primary energy loss is surface recombination of ions, then the conclusion reached above should be valid.

REFERENCES

1. Mickelsen, W. R.: Auxiliary and Primary Electric Propulsion, Present and Future. Journal of Spacecraft and Rockets. November, 1967.

2. Kerslake, W. R., Byers, D. C., and Staggs, J. F.: SERT II Experimental Thruster System. AIAA Paper No. 67-700. September, 1967.

3. Bechtel, R. T.: Discharge Chamber Optimization of the SERT II Thrustor. AIAA Paper No. 67-668. September, 1967.

4. Sohl, G., Wood, K. G., Dillon, T. R., and Vernon, R.: Performance Characteristics of a Cesium Bombardment Ion Engine with a Self-Rectifying Discharge and Automatic Controls. AIAA Paper No. 67-666. September, 1967.

5. Sohl, G., Speiser, R. C., and Wolters, J. A.: Life Testing of Electron-Bombardment Cesium Ion Engines. AIAA Paper No. 66-233. March, 1967.

6. Free, B. A., and Mickelsen, W. R.: Plasma Separator Thruster. Journal of Spacecraft and Rockets. October, 1967.

7. Masek, T. D.: Plasma Characteristics of the Electron Bombardment Ion Engine. Second International Conference on Electron and Ion Beam Science and Technology. April 19, 1966.

8. Kaufman, H. R.: Electron Diffusion in a Turbulent Plasma. NASA TN D-1324. 1962.

9. Gryzinski, Michal: Classical Theory of Electronic and Ionic Inelastic Collisions. Phys. Rev., vol. 115, no. 2, pp. 374-383, July 15, 1959.

10. Gryzinski, Michal: Classical Theory of Atomic Collisions. I. Theory of Inelastic Collisions. Phys. Rev., vol. 138, no. 2A, pp. 336-358, Apr. 19, 1965.

11. Dugan, J. V., Jr., and Sovie, R. J.: Volume Ion Production Costs in Tenuous Plasmas: A General Atom Theory and Detailed Results for Helium, Argon, and Cesium. NASA TN D-4150. September, 1967.

12. Massey, H. S. W., and Burhop, E. H. S.: Electronic and Ionic Impact Phenomena. Oxford Press. 1956.

13. Biberman, L. M., and Norman, G. E.: Continuous Spectra of Atomic Gases and Plasma. Soviet Physics Uspekhi, vol. 10, p. 52. July-August, 1967.

14. Anderson, R. J., Lee, E. T. P., and Lin, C. C.: Electron Excitation Functions of Mercury. Physical Review, vol. 157, no. 1, p. 31. 5 May 1967.

15. Frisch, S. E., and Klucharyov, A. N.: The Role of Cascade Transitions in the Excitation of the 6s7s $^3S_1$ Level of Mercury. Optics and Spectroscopy, vol. 22, no. 2, p. 92. February, 1967.

16. Marr, G. V.: Proc. Phys. Soc., vol. A68, p. 544. 1955.

17. Arnot, F. L., and Baines, G. O.: Elastic and Inelastic Cross Sections of the Mercury Atom. Proc. Roy. Soc., vol. A151, p. 256. 1935.

18. Kaufman, H. R.: An Ion Rocket with an Electron-Bombardment Ion Source. NASA TN D-585. January, 1961.

19. Nolan, J. F., and Emmerich, N. S.: Electron Collision Cross Sections in Metal Vapors. NASA CR-54474 (Westinghouse Electric Company Rep. No. 65-1E5-MHDIN-R1). August 19, 1965.

20. Brink, G. O.: Absolute Ionization Cross Sections of the Alkali Metals. Phys. Rev., vol. 134, p. 345. April 20, 1964.

21. McFarland, R. H., and Kinney, J. D.: Absolute Cross Sections of Lithium and Other Alkali Metal Atoms for Ionization by Electrons. Phys. Rev., vol. 137, p. 1058. February 15, 1965.

22. McFarland, R. H.: Electron-Impact Ionization Measurements of Surface-Ionizable Atoms. Phys. Rev., vol. 159, no. 1. 5 July 1967.

23. Weissler, G. L.: Photoionization in Gases and Photoelectric Emission from Solids. Handbuch der Physik, vol. 21. Springer. 1956.

24. Zapesochnyi, I. P., and Shimon, L. L.: Effective Excitation Cross Sections of Alkali-Metal Atoms Colliding with Slow Electrons. V. Resonance Levels. Jour. of Optics and Spectroscopy. Vol. XXI, no. 3, p. 155. September, 1966.

25. Zapesochnyi, I. P., and Shimon, L. L.: Effective Excitation Cross Sections of Alkali-Metal Atoms Colliding with Slow Electrons. IV. Cesium. Jour. of Optics and Spectroscopy. Vol. 20., p. 421. June, 1966.

26. Korchevoi, Yu, P., and Przonski, A. M.: Effective Electron Impact Excitation and Ionization Cross Sections for Cesium, Rubidium, and Potassium Atoms in the Pre-Threshold Region. Soviet Physics JETP, Vol. 24, no. 6., p. 1089. June, 1967.

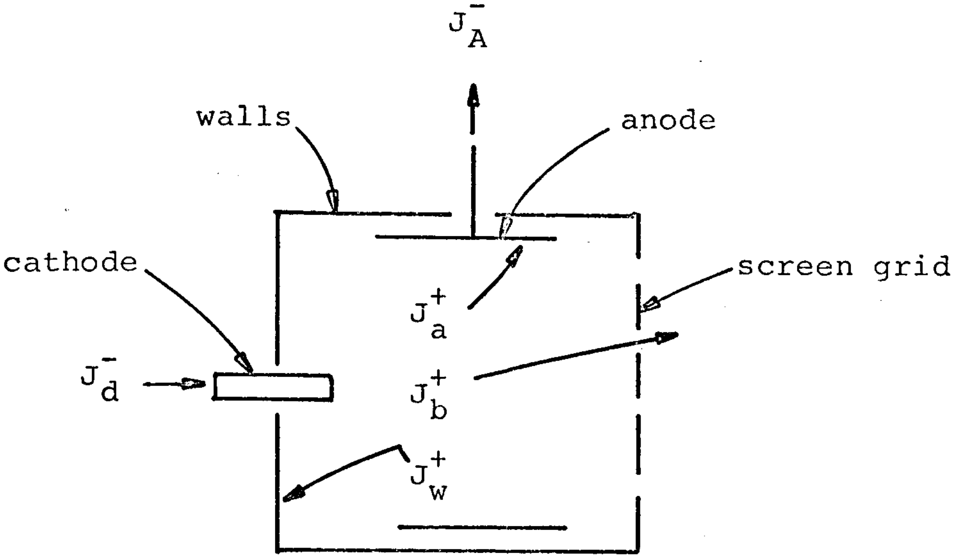

$$J^+ = J_a^+ + J_b^+ + J_w^+$$

$$J_A^- = J_d^- + J_i^- - J_{ar}^-$$

$$J_d^- = J^+ + J_T^-$$

FIG. 3.1. - Fundamental ion and electron currents in bombardment thrusters.

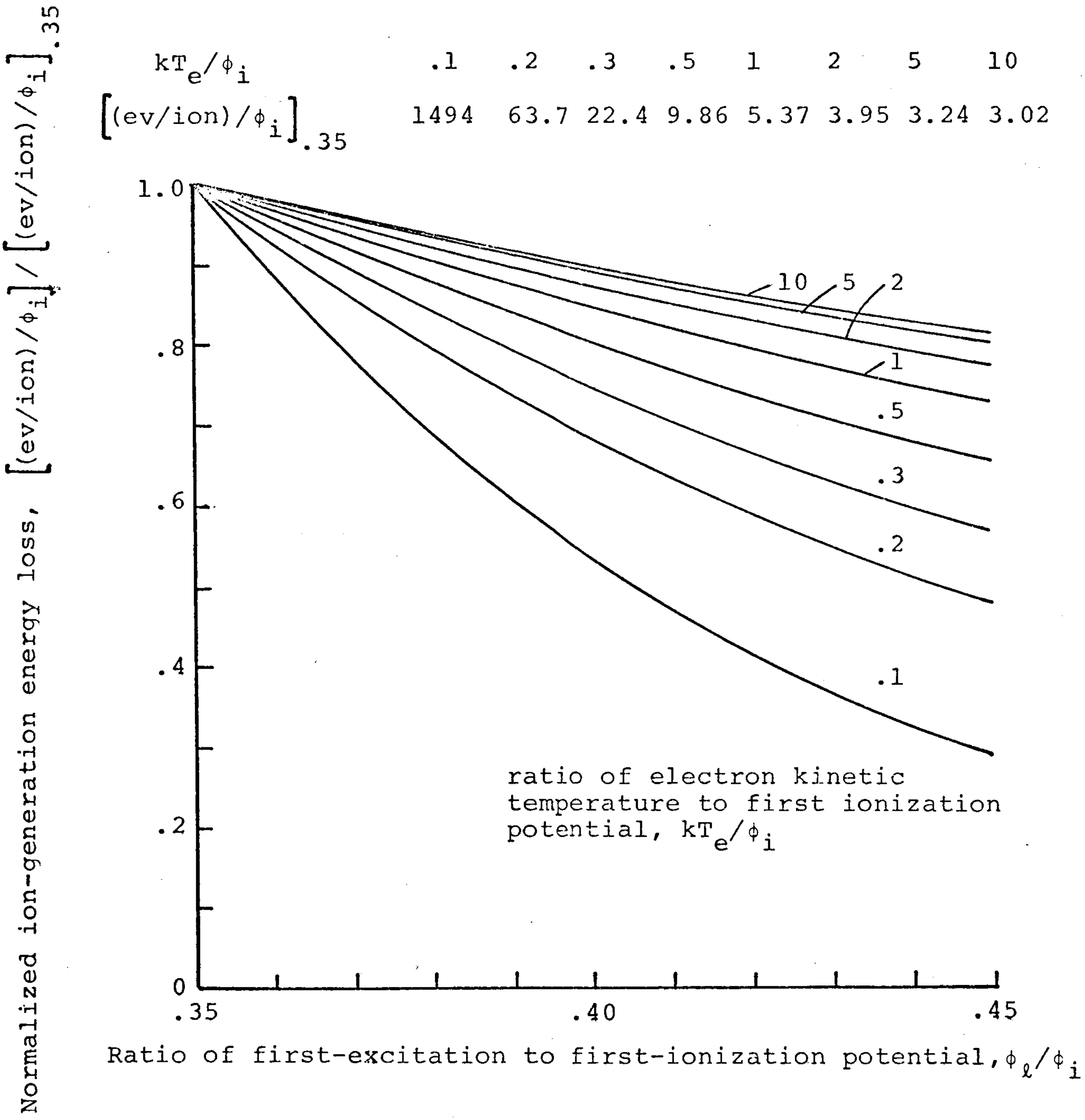

kT_e/ϕ_i	.1	.2	.3	.5	1	2	5	10
$\left[(\text{ev/ion})/\phi_i\right]_{.35}$	1494	63.7	22.4	9.86	5.37	3.95	3.24	3.02

FIG. 3.2. - Normalized ion-generation energy loss calculated from a general-atom theory.

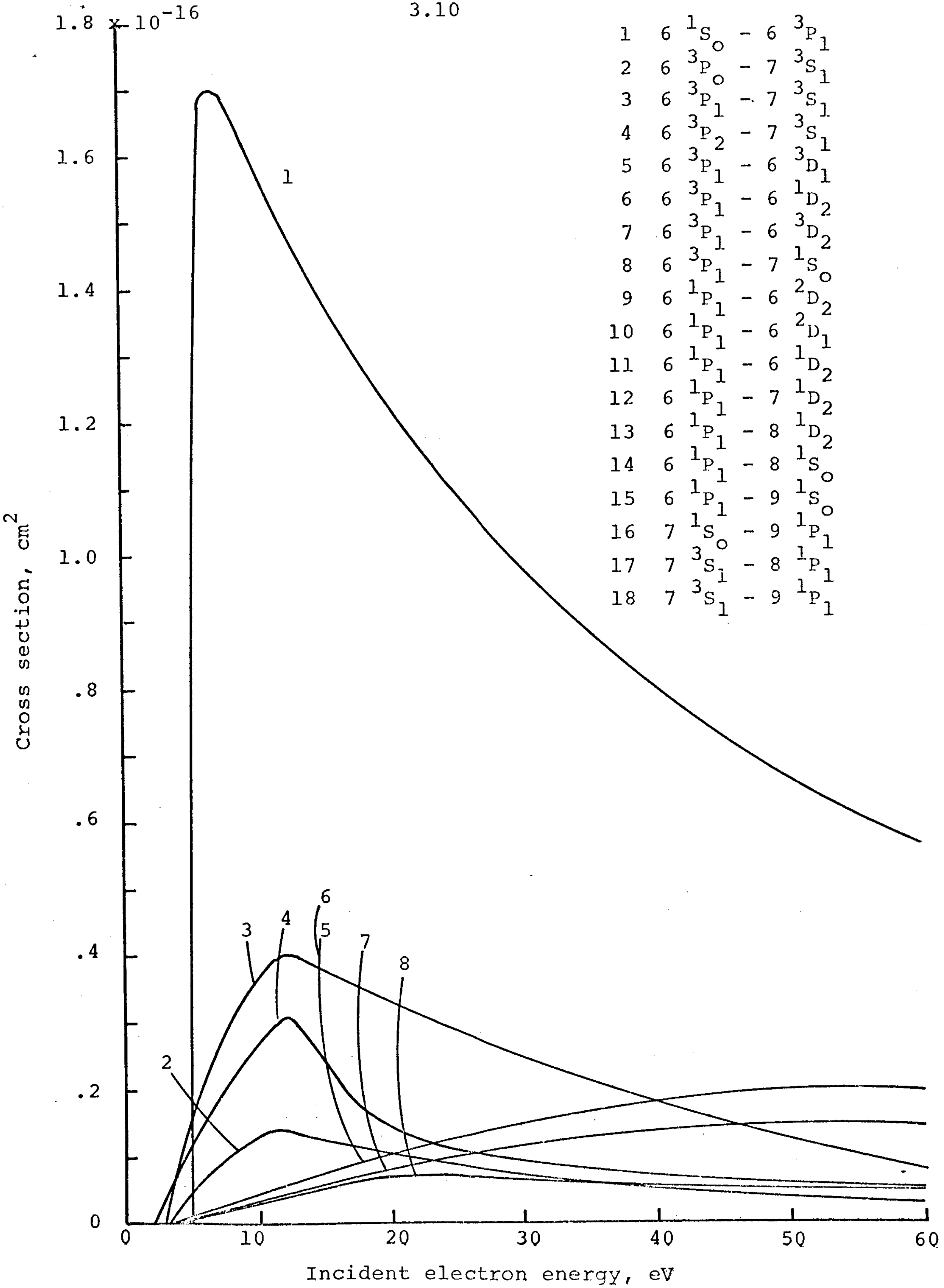

FIG. 3.3. - Excitation cross sections for mercury

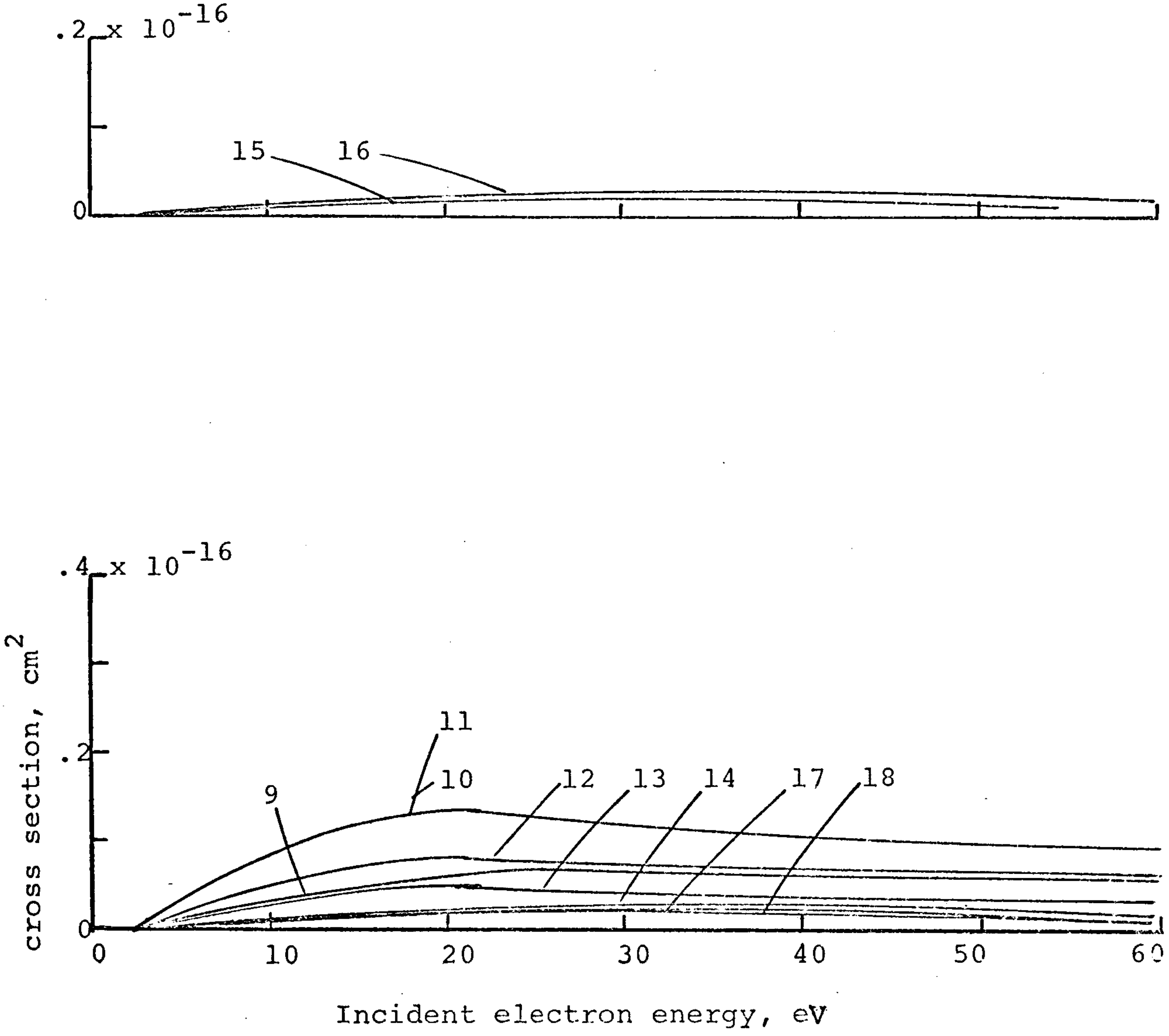

FIG. 3.3. - continued.

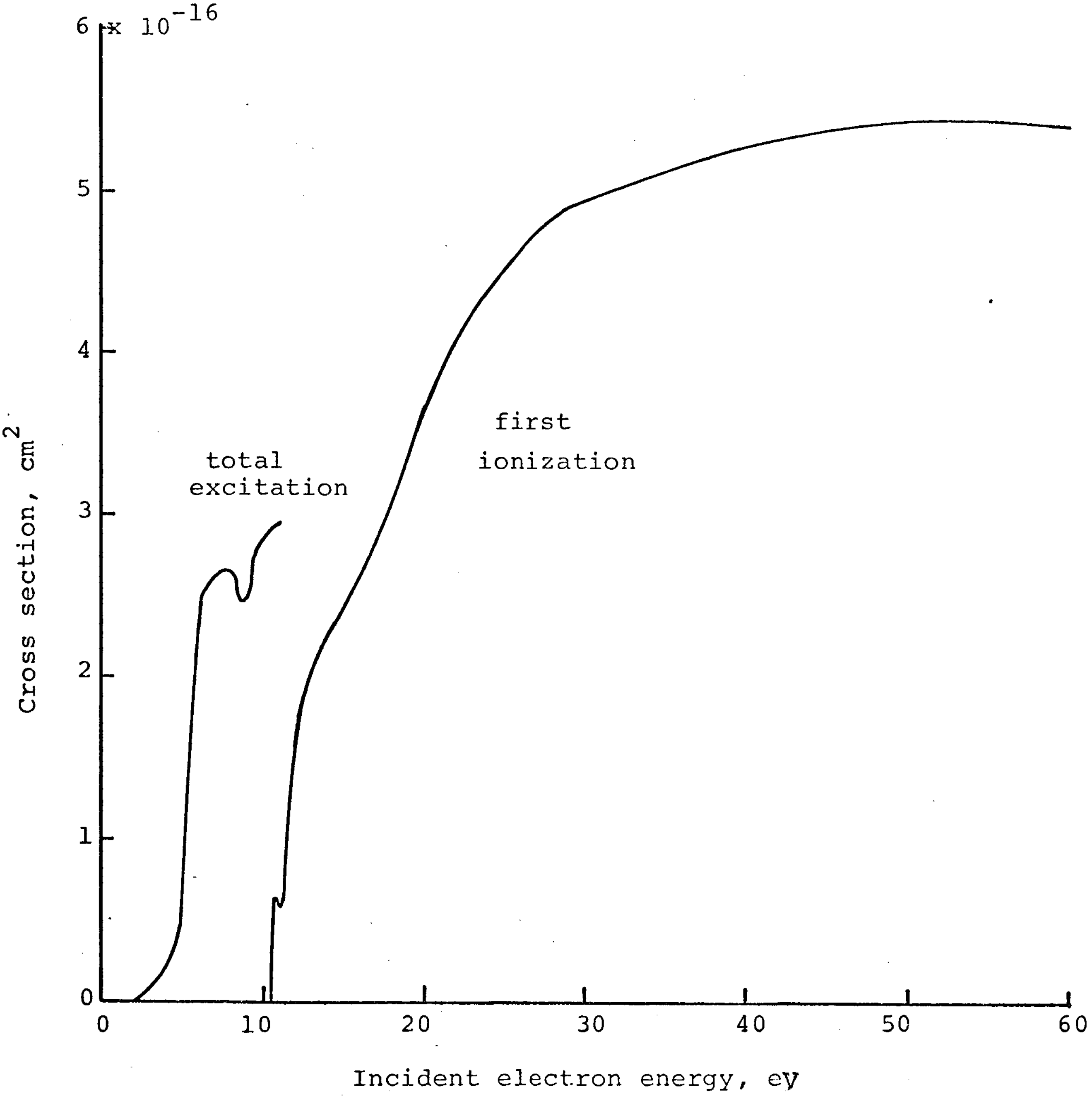

FIG. 3.4. - Total-excitation and first-ionization cross sections for mercury.

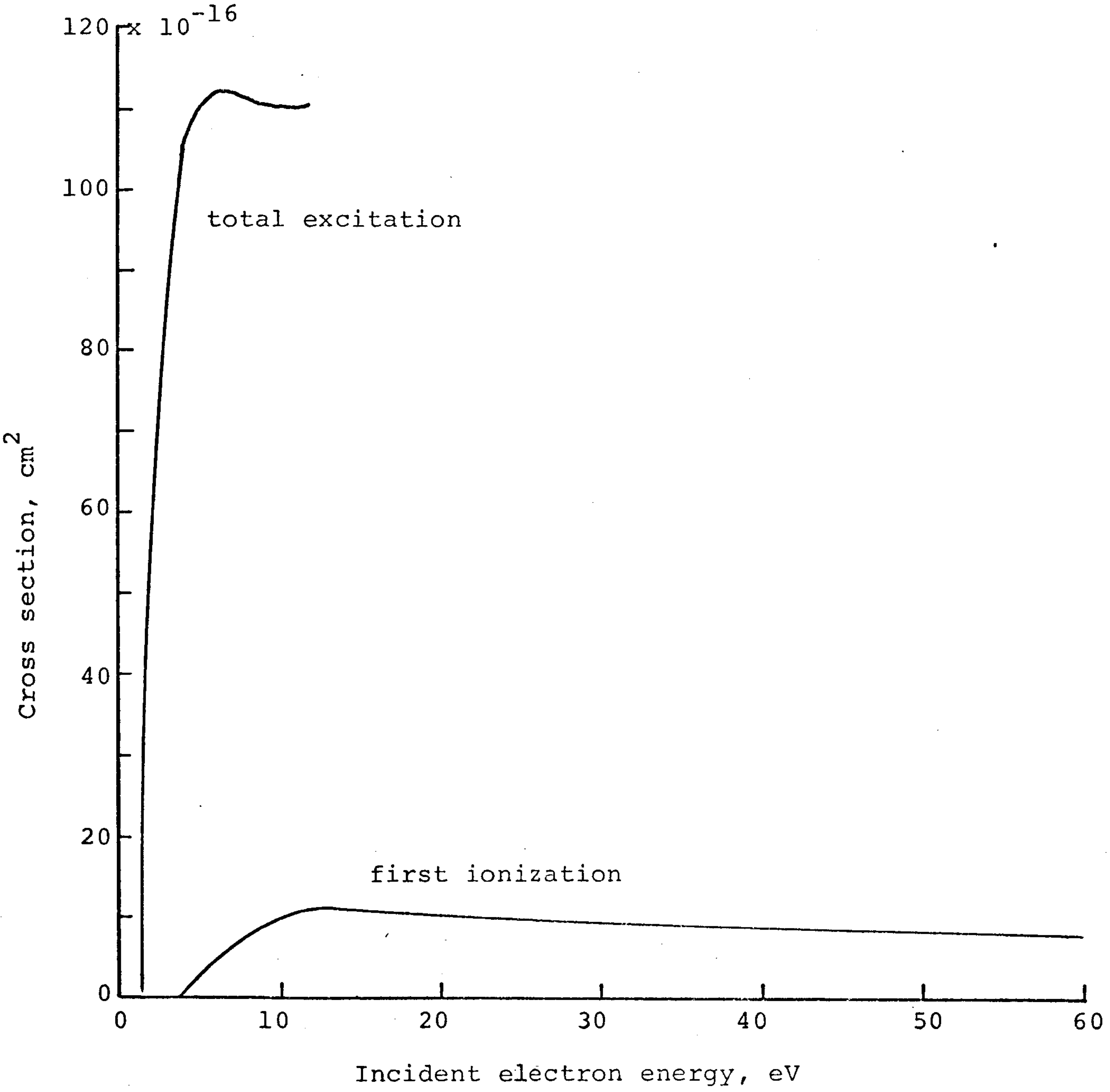

FIG. 3.5. - Total-excitation and first-ionization cross sections for cesium

MEASUREMENT OF NEUTRAL-ATOM SPEED IN BOMBARDMENT THRUSTERS

by Rodney T. Hodgson and Richard Moore

The existence of high speed neutral atoms in an electron bombardment thruster could explain the high cost of ionizing each neutral atom.[4.1,4.2] In order to test the theory, an experiment was started to detect high speed neutral particles in the discharge chamber of a mercury electron bombardment thruster.[4.1]

In essence, the experiment consists of letting neutral particles escape from a hole in the ionization chamber, and counting those that pass through a velocity selector. The velocity selector consists of an aluminum cyliner rotating at high speeds with grooves cut in the outside. See Figure 4.1. Those neutral particles that can pass from one end to the other of the cylinder groove in a time short compared to the time taken for the cylinder to rotate a few degrees will pass through into the ionization gage and be counted. Those particles that are too slow will hit the walls of the grooves and be re-evaporated with a diffuse pattern, thereby greatly reducing the probability of entering the ionization gage.

The thruster (Fig. 4.2) has been set up and operated with arc currents and voltages up to 3 amps and 30 volts. No high voltage has been applied to the accelerating screen of the thruster because the background pressure in the tank is too high without operating the diffusion pump which requires liquid nitrogen.

Highly stabilized and smoothed current supplies have been acquired for the arc, magnetic field, and cathode heater. In this way, the 60 cycle interference has been made as small as possible.

The exit hole for the neutral particles has been mounted in the thruster as shown in Figures 4.3, and 4.4. A fine mesh stainless steel screen connected to the anode will stop electrons from passing if the mesh size is smaller than the Debye length characterizing the plasma at the wall. Another screen is insulated so that it may be positively charged with respect to the anode to repel the ions. The neutral particles that escape both screens then pass through to the velocity selector.

The velocity selector is driven directly from the motor with a flexible coupling formed by a length of 13 gauge piano wire. Too much power would be lost in the original great drive, and too many lubrication problems arose to use gears in a vacuum.

Upon advice from vacuum lubrication specialists at Ball Brothers, Boulder, the bearings of the velocity selector have been lubricated with micro-size molybdenum from Alpha Molycoat Corporation. With this lubrication, the velocity selector has been run for periods up to 15 minutes at speeds of 10,000 R.P.M. The motor runs at 1/3 its rated current of 180 ma at this speed.

A small motor and chopper wheel (Fig. 4.1) has been mounted on the velocity selector to interrupt the neutral particles flux. A photocell and light combination gives a signal in phase with the off time of the particle beam. This signal will be used as a reference by a P.A.R. HR8 lock-in-amplifier connected to the output of the Bayard-Alpert ion gauge used as a detector.

Highly smoothed current sources have been acquired for the ion gauge filament heaters and arc current supply.

References

4.1. Advanced Electric Propulsion Research Semi-Annual Report for the period January to July 1967, NASA Grant NGR06-002-032.

4.2. Knauer, W., Hagen, G., Gallagher, H., and Stack, E.: Investigation of the Discharge in Electron Bombardment Thrusters. AIAA Paper No. 66-244, March, 1966.

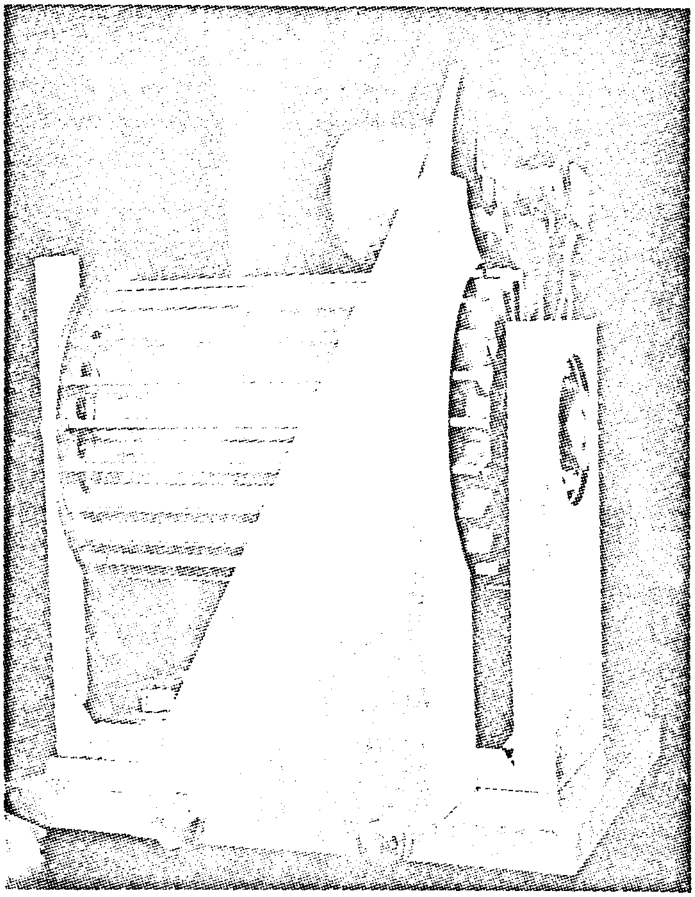

FIG. 4.1. Velocity Selector

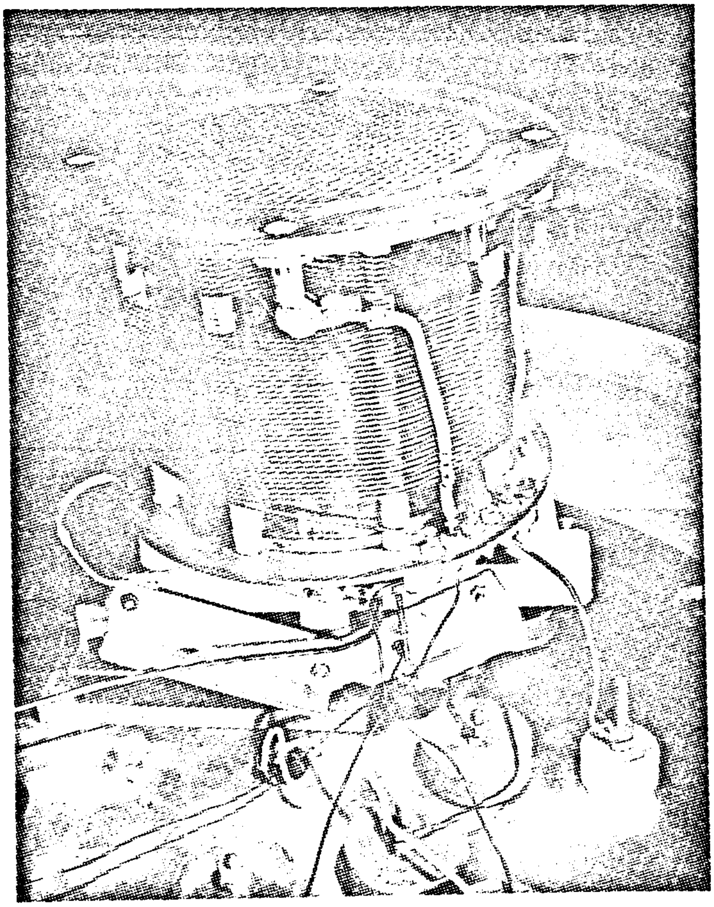

FIG. 4.2. Mounted Thruster

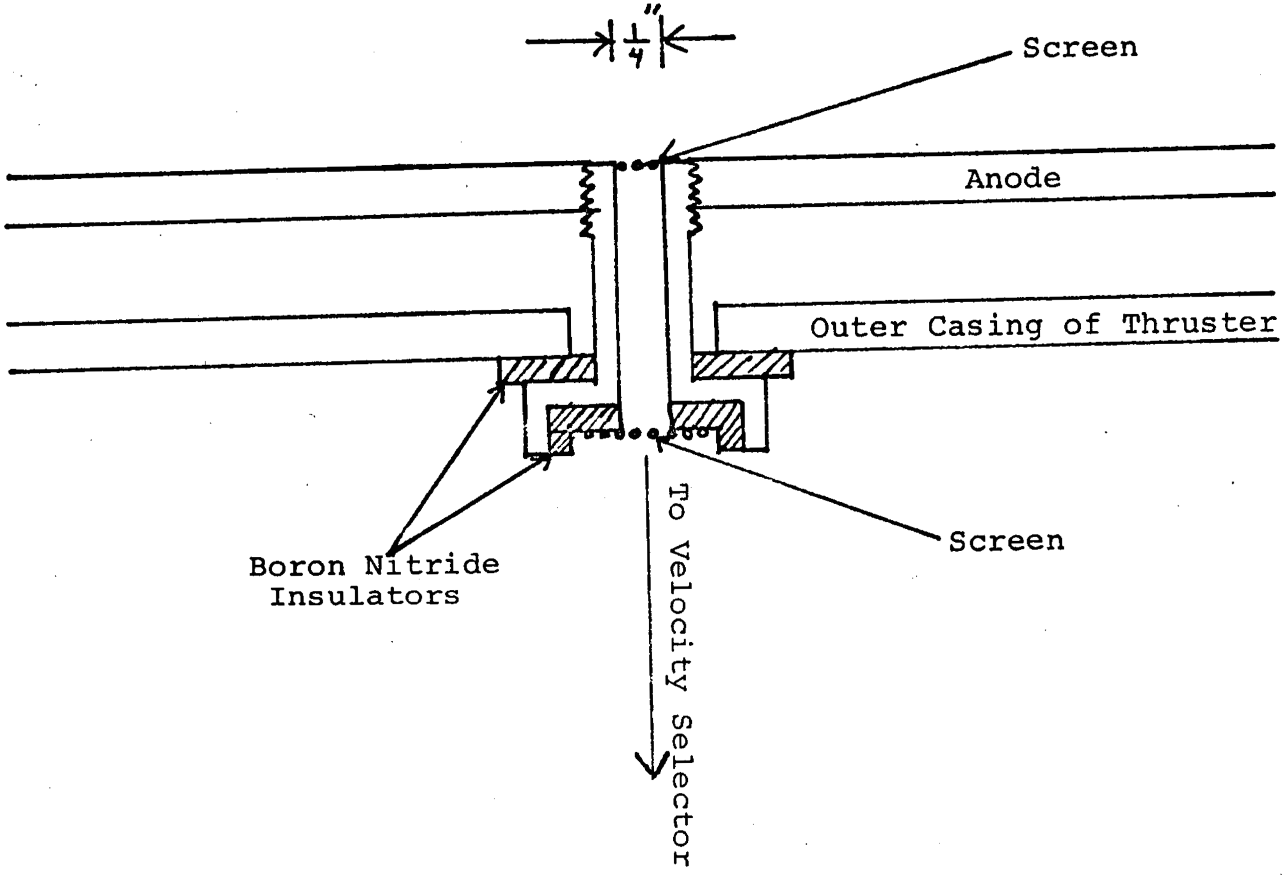

FIG. 4.3. - Schematic Diagram of the 1/4" Hole in Thruster Wall.

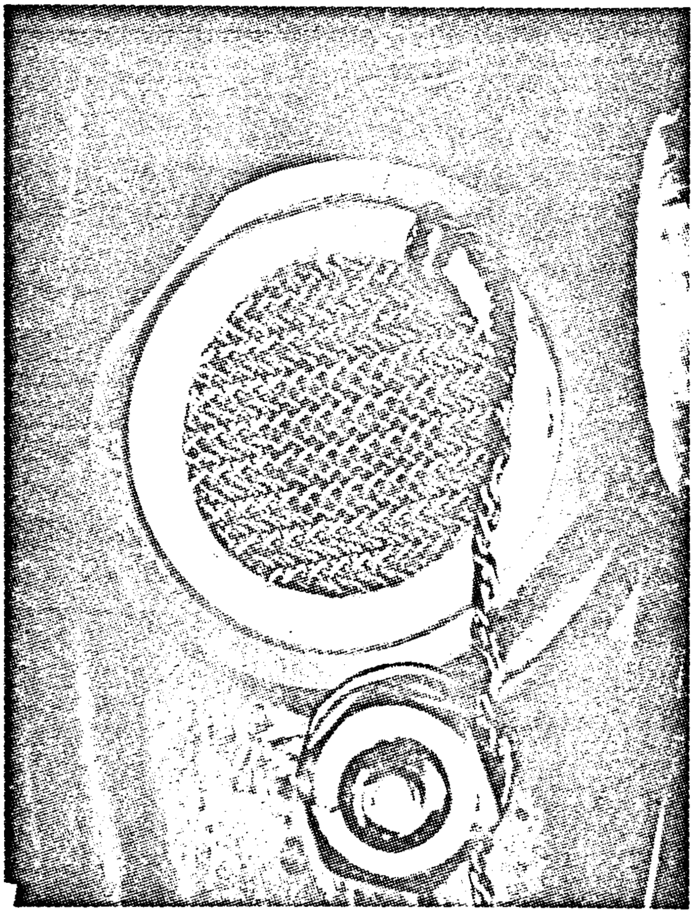

FIG. 4.4. 1/4" Exit Hole for Neutral Particles

STUDY OF HEAT ADDITION TO SUPERSONIC NOZZLES

by Harry I. Leon, Fariborz P. Saheli, and
William R. Mickelsen

INTRODUCTION

The results of this study show that it is possible to have a great increase in the exit velocity of a supersonic nozzle by the addition of heat in the supersonic portion of the nozzle. This increase of velocity is highly desirable for increasing the specific impulse of electric thrusters. This concept could also be used for increasing power and voltage of direct conversion devices of the type shown in Section 8 of Reference 5.1. The heat source is not specified in this study but possible sources include electrical, chemical or condensation such as explained in Section 7 of Reference 5.1.

In a supersonic nozzle without heat addition, the maximum velocity is limited by the stagnation temperature in the plenum. (The maximum gas exit velocity for a standard nozzle using plenum stagnation heat only is shown in Figure 5.1.)

However, when additional heat is added in the nozzle in the flow region, the exit velocity is limited only by the amount of heat added and the nozzle size. Studies to date have shown that it is possible to increase the exit velocity of the nozzle by a factor of 3 or more above that of a nozzle without heat addition without increasing the static temperature in the nozzle. It is possible thereby to increase the specific impulse without inducing high power losses due to ionization of the gas.

This study has been directed toward finding the nozzle geometry and heat addition profile that will give the greatest increase in velocity for the least amount of heat addition and smallest area change. Three methods of approach were used in analyzing the problem:

1. A computer program was developed that is capable of analyzing the velocity and temperature changes in a

nozzle for any heat addition rate or nozzle area change.* Many combinations of heat addition and area changes were studied. The results to date from this code are included in the RESULTS section of this report.

2. Computer programs were developed that would compute the velocity and temperature changes in a nozzle for an area change and a heat input that would result in:
    a. Constant static temperature
    b. Constant Mach number
    c. Constant velocity.

   These programs were initially developed as a check program for the general program given in 1 above, but were found to give many interesting results which are included in this report.
3. After studying the results given from the programs mentioned above, it was clear that the velocity increase in the nozzle was only a function of the amount of heat that was added and the static temperature of the gas,+ but the area ratio required for this velocity is very sensitive to the path in which the heat is added and its relationship with the area change. A computer program is being developed that will optimize the path of the area changes and heat addition to obtain the maximum exit velocity for the smallest heat input and area. Codes developed in 1 and 2 above will not only serve to give an initial design, from which this code will optimize by a process of iteration, but will also serve as a check on the output.

---

[*] The computer codes listed in 1 and 2 worked equally well in the supersonic or subsonic portion of the nozzle. However, the computer code 1 was found unstable in the Mach number region between 1.00 to 1.05.

[+] This is of course assuming no discontinuities or friction losses are in the flow.

THEORETICAL ANALYSIS

The Velocity in a Supersonic Nozzle without Heat Addition in Flowing Section

The principle of the conservation of energy may be written for an adiabatic flow process between any points 1 and 2. In the energy equation the decrease in enthalpy, h, is equal to the increase in kinetic energy of the flowing gases:

$$h_1 - h_2 = \frac{1}{2} (v_2{}^2 - v_1{}^2) \qquad (5.1)$$

Assuming a perfect gas:

$$\Delta h = C_p \ \Delta T \qquad (5.2)$$

the specific heat at constant pressure, C_p, can be rewritten in terms of the ratio of the specific heats, γ, and the gas constant, R giving:

$$C_p = \frac{\gamma}{\gamma - 1} \ \frac{R}{m} \qquad (5.3)$$

where m is the molecular (or atomic) weight of the gas.

For an adiabatic, isentropic nozzle the energy equation may be written as:

$$\frac{V^2}{2} + h = h_o = \text{constant} \qquad (5.4)$$

where h_o is the stagnation enthalphy. Using equations (5.2), (5.3), and the steady-state energy equation (5.4), the flow velocity, V, can be solved in terms of the stagnation temperature, T_o, and the static temperature, T:

$$V = \sqrt{\frac{2\gamma}{\gamma - 1} \frac{R}{m} (T_o - T)} \qquad (5.5)$$

Equation (5.5) is the relationship between the velocity in the nozzle and the stagnation and static temperatures of the gas. Thus for a gas heated only in the plenum region, the maximum velocity is dependent only on the stagnation temperature, T_o, and the molecular weight of the gas, m. The static temperature, T, can be written in terms of the Mach number, M, and the stagnation temperature T_o. This relationship is given below:

$$T = T_o \left(1 + \frac{\gamma - 1}{2} M^2\right)^{-1} \tag{5.6}$$

This equation (5.6) is very important when the working fluid of the nozzle is a condensible gas. If the gas condenses at the temperature, T, the maximum Mach number, M, that can be obtained is fully determined once the stagnation temperature, T_o, is defined. However, if additional heat is added in the nozzle (as will be shown in the following section), the velocity can be further increased without condensation occurring. From the equation of continuity (in one dimension):

$$\rho_1 A_1 V_1 = \rho_2 A_2 V_2 \tag{5.7}$$

The Mach number, M, which is a function of velocity and static temperature, $M = V \left(\gamma \frac{R}{m} T\right)^{-\frac{1}{2}}$, can be expressed as a function of the nozzle area. This relationship is given below:

$$\frac{A}{A_T} = \frac{1}{M}\left[\left(\frac{2}{\gamma + 1}\right)\left(1 + \frac{\gamma - 1}{2} M^2\right)\right]^{\frac{\gamma + 1}{2(\gamma - 1)}} \tag{5.8}$$

where A_T is the area of the nozzle throat. The gas velocity can be solved for as a function of the stagnation temperature and the nozzle area ratio. This analysis was done for the case of lithium gas and the results are shown on Figure 5.1. It should be noted in Figure 5.1 that the velocity of the lithium does not increase much beyond a velocity of 2310 meter/sec in the case of a stagnation temperature of 2500°K due to condensation of lithium, that will occur around 1600°K.

Velocity in a Supersonic Nozzle when Heat is Added in Supersonic Section

When additional energy is added to the working gas of the nozzle beyond the stagnation region, the physics of the problem become much more difficult. This is especially true when the area of the nozzle is allowed to vary at the same time heat is added. Conventional texts and reference books in compressible fluid flow show that if the area of the supersonic section of a nozzle is held constant when heat is added, the velocity of the flow will be decreased. However, it was found that when the nozzle area was increased at sufficiently large ratio at the same time heat was added, the velocity of the gas increased.

For the general case, the only way to analyze the combined effects of area change and heat addition on the velocity in a supersonic nozzle is by approximate or numerical treatments. A considerable clarification of the numerical calculation and the qualitative interpretation is made possible by manipulation of the conservation equations and other relevant equations, following a method devised by Shapiro and Hawthorne[2]. The following assumptions were made in the analysis:

1. The flow is one dimensional and steady.
2. Changes in stream properties are continuous.
3. The gas is semiperfect, i.e. it obeys Boyle's and Charles' laws and has a specific heat which varies only with temperature and composition. (For the preliminary calculations included in this report the specific heat was held constant.)
4. * Heat is added uniformly across each nozzle station.
5. * The effect of nozzle wall friction is neglected.
6. * There is no change of phase of the gas or chemical reaction.
7. * Gas is neither injected or removed from the stream on its passage through the nozzle.

The method of analysis consists of expressing the differential of the dependent quantity velocity through a linear combination of the independent variables, heat addition and area change. The coefficients of these linear combinations, called the "influence coefficients"** are a function of a single variable - the Mach number. The infinitesimal control surface on which the analysis

---

* Future analysis will be a more general study and will eliminate some of the assumptions (4.) - (7.) made in the present study.

** The coefficients of the independent variables are called "influence" coefficients and prove to be functions of γ and M only.

is based is shown in Figure 5.2 below:

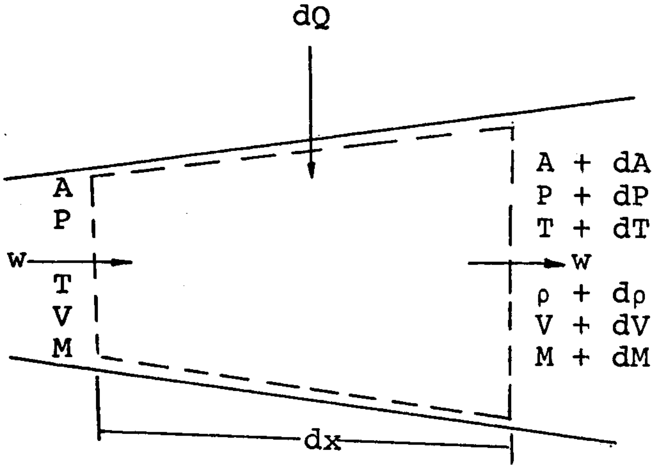

FIG. 5.2. Control Surface for Analysis of Continuous Changes.

The Equations used in the analysis were derived by taking the logarithmic differentiation of the following relations.

Equation of Static

$$P = \rho \frac{R}{m} T \tag{5.9}$$

Taking logarithms differential of equation (5.9):

$$\frac{dp}{P} = \frac{d\rho}{\rho} + \frac{dt}{T} - \frac{dm}{m} \tag{5.10}$$

Sound Velocity

$$c^2 = \gamma\ R/m\ T \tag{5.11}$$

Taking logarithmic differential gives:

$$\frac{dc}{c} = \frac{1}{2}\left(\frac{d\gamma}{\gamma} + \frac{dT}{T} - \frac{dm}{m}\right) \tag{5.12}$$

Defination of Mach Number

$$M^2 = V^2/c^2 = V^2 m/\gamma RT \tag{5.13}$$

Taking logarithmic differential of (5.13):

$$\frac{dM^2}{M^2} = \frac{dV^2}{V^2} + \frac{dm}{m} - \frac{d\gamma}{\gamma} - \frac{dT}{T} \tag{5.14}$$

Equation of Continuity

$$w = \rho A V \tag{5.15}$$

Taking logarithmic differential of (5.15):

$$\frac{dw}{w} = \frac{d\rho}{\rho} + \frac{dA}{A} + \frac{dV}{V} \tag{5.16}$$

Energy Equation

The energy equation for the control surface may be written in the form:

$$w(dQ) = w(dh) + w(d\,\frac{V^2}{2}) \tag{5.17}$$

Substituting equations (5.2), (5.3), and (5.13) into equation (5.17) and rearranging:

$$\frac{dQ}{C_p T} = \frac{dT}{T} + \frac{\gamma - 1}{2} M^2 \frac{dV^2}{V^2} \tag{5.18}$$

Momentum Equation

For steady-flow problems, Newton's second law of motion is most conveniently applied by equating the net force acting on a control surface to the increase of momentum flux of the streams thru the control surface. Assuming the angle of divergence of the walls is small, and friction is neglected, the momentum equation can be written in the following form:

$$AdP = -\,wdV \tag{5.19}$$

Using equations (5.9) and (5.11) in (5.19) and rearranging:

$$-\frac{dP}{P} = \frac{KM^2}{2} \frac{dV^2}{V^2} \tag{5.20}$$

Stagnation Temperature

With the assumption of constant specific heat, C_p, and constant molecular weight, m, the stagnation temperature, T_o, may be expressed as:

$$T_o = T + \frac{V^2}{2C_p} \tag{5.21}$$

By substituting the definition of the Mach number, M, given in equation (5.13), and the perfect gas law, equation (5.9), into equation (5.21), the equation can be rewritten in terms of its "influence coefficient", which is previously derived in equation (5.6):

$$T_o = T\left(1 + \frac{\gamma - 1}{2} M^2\right) \tag{5.22}$$

Stagnation Pressure

The relationship between pressure and temperature for an isentropic process of a perfect gas is:

$$\frac{T}{T_o} = \left(\frac{P}{P_o}\right)^{\frac{\gamma - 1}{\gamma}} \tag{5.23}$$

Therefore, using equation (5.22), the relation between the static temperature, T, and the stagnation temperature, T_o, can be written as:

$$\frac{P}{P_o} = \left(1 + \frac{\gamma - 1}{2} M^2\right)^{\frac{\gamma - 1}{\gamma}} \tag{5.24}$$

Working Equations

Using the usual methods of solving systems of simultaneous, linear algebraric equations, equations (5.10), (5.14), (5.18), and (5.20) can be solved in terms of the following independent and dependent variables:

Independent	Dependent
dA/A, dT_o/T_o	dM^2/m, dV/V, dT/T

These equations are listed below:

$$\frac{dM^2}{M^2} = -2\,\frac{\left(1 + \frac{\gamma-1}{2} M^2\right)}{1 - M^2}\,\frac{dA}{A} + \frac{\left(1 + \gamma M^2\right)\left(1 + \frac{\gamma-1}{2} M^2\right)}{1 - M^2}\,\frac{dT_o}{T_o} \tag{5.25}$$

$$\frac{dV}{V} = -\frac{1}{1-M^2}\frac{dA}{A} + \left(1 + \frac{\gamma-1}{2}M^2\right)\frac{dT_o}{T_o} \qquad (5.26)$$

$$\frac{dT}{T} = \frac{(\gamma-1)M^2}{1 - M^2}\frac{dA}{A} + \frac{(1 - \gamma M^2)(1 + \frac{\gamma-1}{2}M^2)}{(1 - M^2)}\frac{dT_o}{T_o} \qquad (5.27)$$

Thus, in equations (5.25), (5.26), and (5.27), the changes in the Mach number, area ratio and static temperature were related to the changes in the nozzle area ratio and the stagnation temperature.

In the following section of this report, it is explained how the equations given in this section were used in the analysis.

METHOD OF ANALYSIS

The analysis was made by CDC6400 digital computer from codes written in Fortran IV. Five computer programs were written to solve the following conditions of heat addition to a supersonic nozzle. The codes computed the following:

Code 1: heat addition and area change with the supersonic gas in the nozzle maintaining a constant Mach number.

Code 2: heat addition and area change in the nozzle to maintain a constant static temperature of the fluid.

Code 3: heat addition and area change required for the gas to maintain a constant velocity in the nozzle.

Code 4: velocity and area change for the flow in a supersonic nozzle without heat addition.

Code 5: general program for computing the effects of area changes and heat addition along any path.

The basic equations and iteration methods used in these codes will be explained below.

When a path of heat addition is predetermined as in the case of codes 1 thru 4, the equation of the velocity can be integrated in closed form. The velocity can be determined by either the use of equation (5.21) or (5.22) written in the following forms:

$$\frac{T_{02}}{T_{01}} = \frac{T_2}{T_1} \frac{(1 + \frac{\gamma-1}{2} M_2^2)}{(1 + \frac{\gamma-1}{2} M_1^2)} \tag{5.22a}$$

$$\frac{T_{02}}{T_{01}} = \frac{T_1 + V_1^2/2C_p}{T_2 + V_2^2/2C_p} \tag{5.21a}$$

The use of the stagnation temperature ratio, T_{02}/T_{01} for the measure of heat imput was found very convenient since at the start of heat input the ratio would be one and the code would increase this ratio by small steps and obtain the solution on each increment. The actual amount of heat input, Q, is a function of the stagnation temperature ratio, the initial stagnation temperature, T_{01}, the specific heat, and the weight flow rate as shown in the expression below:

$$Q = wC_p \quad (T_{02} - T_{01}) \tag{5.28}$$

which can be rewritten in the following form:

$$\frac{T_{02}}{T_{01}} = \frac{Q}{(wC_p)T_{01}} + 1 \tag{5.28a}$$

It now will be shown how the velocity, static temperature and area ratio were determined in the analysis.

Constant Mach number case, Code 1.

With the path of constant Mach number, equation (5.22a) reduces to:

$$\frac{T_{02}}{T_{01}} = \frac{T_2}{T_1} \tag{5.29}$$

Since the Mach number is known, $M_2 = M_1$, and the static temperature is known once the heat input is given, the velocity at point (2) can be determined using equation (5.13) written in the following form:

$$V_2 = M_2 \quad (\gamma \cdot \frac{R}{m} \cdot T_2) \tag{5.13a}$$

The area ratio required for the constant Mach number path was determined by integration of equation (5.25) with dM^2 set equal to zero. Integrating equation (5.25) gives the expression for area ratio, A_2/A_1 as a function of stagnation temperature ratio as shown below:

$$\frac{A_2}{A_1} = \left(\frac{T_{02}}{T_{01}}\right)^{\frac{1 + \gamma M^2}{2}} \qquad (5.30)$$

Constant velocity case, Code 2.

The velocity in this case is easily solved for by use of equation (5.21a), where the value of $V^2/2C_p$ is a known constant, say equal to B. Thus the static temperature can easily be determined from the resulting equation:

$$\frac{T_{02}}{T_{01}} = \frac{T_1 + B}{T_2 + B} \qquad (5.21b)$$

The area ratio in the case was solved for by integrating equation (5.26) with dV = 0. This gives the following equation for the area ratio:

$$\frac{A_2}{A_1} = \left(\frac{T_{02}}{T_{01}}\right)^{1 + \frac{\gamma-1}{2} \bar{M}^2} \qquad (5.31)$$

where $\bar{M}$ is the average Mach number between area A_1 and A_2 defined as*

$$\bar{M} = \frac{M_1 + M_2}{2} \qquad (5.32)$$

where M_2 is determined using equation (5.13a)

---

* Since the average Mach number is assumed a linear average between M_1 and M_2 the size of increments were required to be small in order to keep the errors very small.

Constant static temperature case, Code 3.

In this case it is easier to first solve for the M_2 using equation (5.22a) since all the other variables are known. Using this value of M_2 and since $T_1 = T_2$, the velocity, V_2, was determined using equation (5.13a).

The area ratio for this path is determined by integrating equation (5.27) with $dT = 0$, giving the relationship:

$$\frac{A_2}{A_1} = \left(\frac{T_{02}}{T_{01}}\right)^{\frac{(\gamma\bar{M}^2 - 1)(1 + \frac{\gamma-1}{2}\bar{M}^2)}{(\gamma-1)\bar{M}^2}} \qquad (5.33)$$

Constant stagnation temperature, Code 4.

For this analysis, the Mach number was varied in increments starting at zero. The static temperature was then determined by equation (5.22) and the velocity by equation (5.13a). The area ratio corresponding to the Mach number was determined using equation (5.8).

General program, Code 5.

This code did the analysis of the heat addition along any path. Since the path was not defined, the velocity had to be obtained by integrating equation (5.26) using numerical methods. In order to accomplish this, equation (5.26) was written in finite difference form shown below:

$$\frac{V_2}{V_1} = \left[\frac{A_2}{A_1} - 1 - \left(1 + (\frac{\gamma-1}{2})\bar{M}^2\right)\left(\frac{T_{02}}{T_{01}} - 1\right)\right]\left[\frac{1}{\bar{M}^2 - 1}\right] + 1 \qquad (5.34)$$

The value of the area ratio, $AR = A_2/A_1$, was initialized at 1.0 and increased in small steps, called DAR, where DAR was found to give good results when a value of .001 was chosen. Thus the area change for each step was written as:

$$AR = AR + DAR \qquad (5.35)$$

The stagnation temperature ratio, $TR = T_{02}/T_{01}$, for each step was then allowed to vary as a function of the area ratio, AR, by many paths. The two paths that gave the best results are listed below:

$$TR = TR + C(AR) \tag{5.36}$$

and

$$TR = AR/C + (C-1)/C \tag{5.37}$$

C in the above equations is a constant which was varied in the imput of the program. For the programs using equation (5.36), C was found to have a range of interest between 0.01 and 0.60 and for the program using equation (5.37) the value of C was varied between 2 to 20. However, since the use of either equation (5.36) or (5.37) the temperature ratio, TR, is basically a linear function of the area ratio, AR, the results gave good correlation with each other and were able to be plotted on a common constant temperature curve as shown on Figures 5.3 and 5.4.

Returning back to how equation (5.34) was solved - the initial condition at each point was known which included the value of the initial Mach number M_1. It was necessary to solve for the average Mach number of each interval by a process of iteration. An initial guess of the value of M_2 was $M_2 = M_1$. The velocity, V_2, was then obtained and using V_2, the static temperature, T_2, was obtained from equation (5.21). Then knowing the static temperature, T_2, and velocity, V_2, the computed Mach number at the end of the interval, M_{2C}, was determined using equation (5.13). If the difference between the initial guess of the Mach number and M_{2C} was greater than 0.000001, a new guess of the exit Mach number, M_{2new} was made using the relationship:

$$M_{2new} = M_{2C}\left(\frac{M_{2old}}{M_{2C}}\right)^{ex} \tag{5.38}$$

where values of 0.5 and 0.25 were used for ex. Using M_{2new}, a new value of the average Mach number was made using equation (5.32), and equation (5.34) was then solved again for the V_2

using the same values of AR and TR. This process was repeated until the difference between the guessed Mach number and the computed Mach number was less than 0.000001, which took on the average of 5 iterations. Once the value of the Mach number converged, the Mach number, static temperature and velocity were printed, and then AR and TR were increased as shown in equations (5.35), (5.36) or (5.37), M_2 was set equal to M_1, and the process was repeated.

The general code also computed the stagnation and static pressure along the nozzle. The value of the static pressure at the start of heating was computed using equation (5.24). The change in static pressure per increment of the heated section of the channel was computed using the relationship below:

$$\frac{P_2}{P_1} = \frac{A_1\, M_1}{A_2\, M_2} \left[\left(\frac{1 + \frac{\gamma-1}{2}\, M_1^{\,2}}{1 + \frac{\gamma-1}{2}\, M_2^{\,2}} \right) \left(\frac{T_{02}}{T_{01}} \right) \right]^{\frac{1}{2}} \qquad (5.39)$$

The change in the stagnation pressure was also computed using the equation below:

$$\frac{P_{02}}{P_{01}} = \frac{P_2}{P_1} \left[\frac{1 + \frac{\gamma-1}{2}\, M_2^{\,2}}{1 + \frac{\gamma-1}{2}\, M_1^{\,2}} \right]^{\gamma/\gamma\, -\, 1} \qquad (5.40)$$

The results of the analysis are given in the next section of this report.

RESULTS

The addition of heat to a supersonic nozzle was found to give an increase in the gas velocity if the area is enlarged at a rate sufficient to accommodate the increase of heat. The comparison of supersonic nozzle exit velocity with and without heat addition is also shown on Figure 5.4. This figure shows that with plenum stagnation temperature of 2500°K, the maximum velocity would be 3700 meter/sec, while when heat was added to the nozzle, exit velocities above 10,000 meter/sec were found possible. When heat is added to supersonic section of the nozzle without an increase in the nozzle area, the flow velocity will decrease. The minimum rate of area change to heat addition to prevent a lowering of the velocity is the constant velocity curve shown on Figure 5.5. In order for the flow velocity to increase with heat addition the area increase, A_2/A_T must be larger than the constant velocity case for the same ratio of the stagnation temperature change, T_{02}/T_{01}.

For a given exit static temperature, the velocity of exit is a function of the heat addition to the gas stream. Figure 5.3 shows the relationship between the exit velocity and the heat imput, T_{02}/T_{01}, and the static temperature. A cross plot of Figure 5.3 is shown on Figure 5.4. The most important results of this study are shown on these two figures. The velocity was found to be a function of only the static temperature and the amount of heat addition, T_{02}/T_{01}. The area change shown on Figure 5.4 is for the case where the area change is a linear function of the heat addition given by equations (5.36) and (5.37) and represents the smallest area ratio found at present for the velocity increase. When the heat addition was not a linear function of the area change, such as in the cases where the heat addition was added in such a manner as to keep velocity, Mach number or static temperature constant, the area ratios required for the velocity increase were found to be very much larger. A comparison of the area ratios required for velocity increases for these paths is shown on Figure 5.5. Studying Figure 5.5, it is clear that the path taken for heat addition has a strong effect on the area ratio required for a given velocity. The mathematical expression describing the relationship between the path of heat addition and the area ratio is still under study.

The effect of the heat addition and area change on the pressure distribution in the nozzle was studied. The static pressure was found to decrease along paths described by equations (5.36) and (5.37). A typical plot of the static pressure is shown on Figure 5.6. The stagnation pressure was found to decrease when heat was added along the same path. This is also shown on Figure 5.6.

CONCLUSION AND RECOMMENDATION FOR FUTURE WORK

The following conclusions can be made from this preliminary study of heat addition to a supersonic nozzle:

1. The heat addition to the nozzle in the supersonic region is capable of increasing the velocity of the exit gas to 3 or more times the velocity possible with a nozzle with heat addition in the plenum only. This velocity increase could be accomplished without the need of raising the static temperature above plenum conditions. For example, the exit velocity of a nozzle using lithium gas could be increased from 4000 meters/sec (400 seconds impulse) with heating only in the plenum, to 10,000 meter/sec (1000 seconds) or more with heating in the supersonic section without excessive static temperatures (see Figure 5.3).
2. The maximum velocity that can be obtained in a plenum-heated nozzle is a function of the stagnation temperature and the molecular weight of the gas, while the maximum velocity that can be obtained in a nozzle heated along the flow passage is a function of the total stagnation temperature that the gas obtains.
3. The nozzle area ratio required for a given velocity with a fixed amount of heat imput is a strong function of the path in which the heat is applied to the nozzle.

For example, for a given velocity, the area ratio required for a path of constant temperature was found to be approximately the square of the area required for a path where the stagnation temperature ratio was kept as a linear function of the area change.

4. The static pressure decreased toward the exit of the nozzle when heat was added and the area was changed along a path that led to a high increase in velocity for relatively small area changes. This decrease in static pressure aids in holding the flow along the wall of the nozzle thus preventing separation.

Future work on this study is recommended to take the following directions in order to develop this concept into a practical design:

1. The actual nozzle geometry will be studied, taking wall friction and heat input sources into account.
2. If a condensating gas is found to be the best working fluid, the effects of this condensating gas on the nozzle design will have to be studied. (See Reference 5.1, Section 7.
3. Additional energy losses in a nozzle due to gas disassociation, shocks, and separations from the nozzle walls will be studied.
4. A test model should be made to study method of heat addition and to prove design concept.

REFERENCES

5.1. Mickelsen, W. R.: Advanced Electric Propulsion Research, Semi-Annual Report for January 1, 1967 to June 30, 1967, prepared for National Aeronautics and Space Administration. Grant NGR06-002-032.

5.2. Shapiro, A. H.: The Dynamics and Thermodynamics of Compressible Fluid Flow, Volume 1, Ronald Press Company. 1953.

5.3. Sutton, G. P.: Rocket Propulsion Elements, Third Edition, 1963, Wiley Book Company.

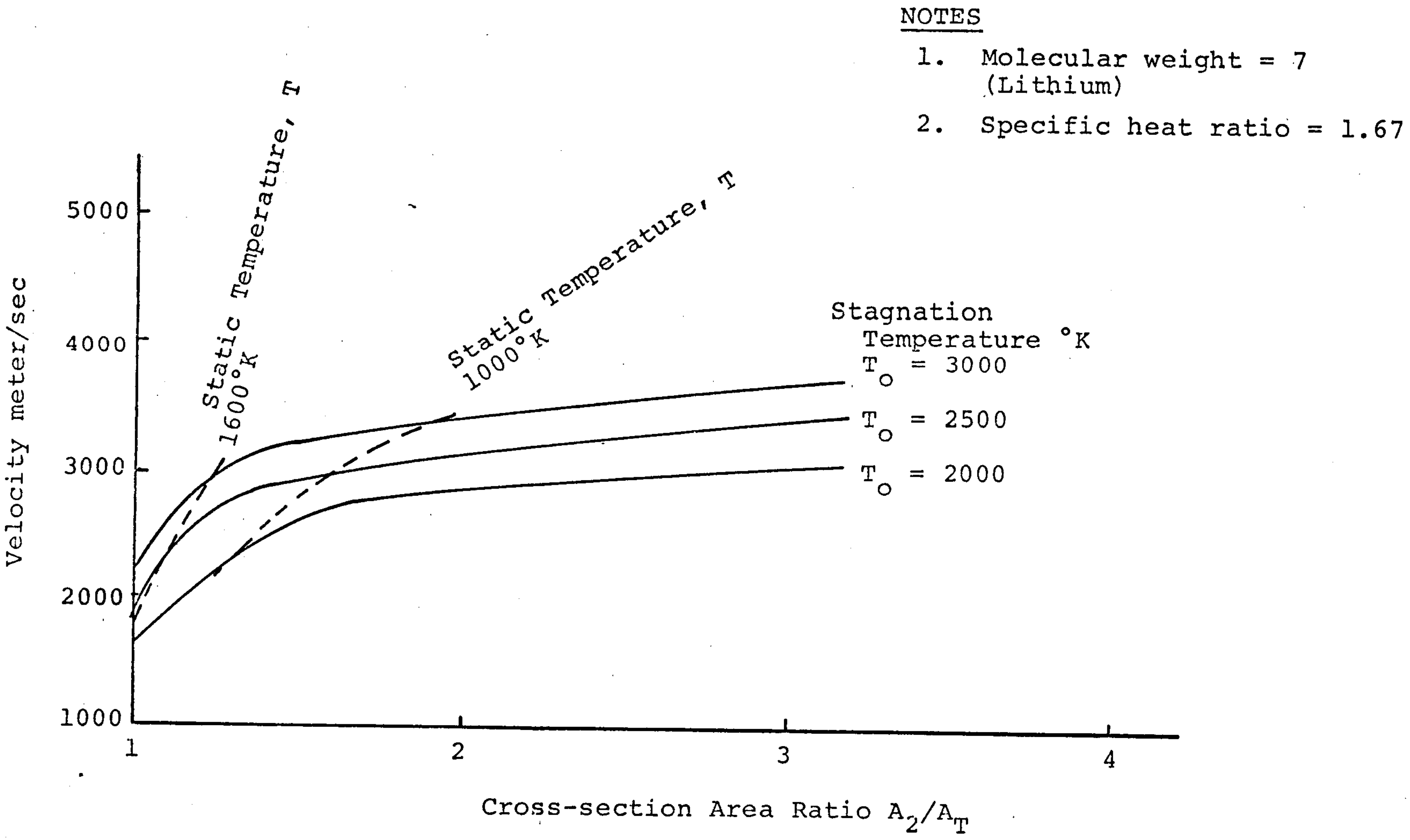

NOTES

1. Molecular weight = 7 (Lithium)
2. Specific heat ratio = 1.67

FIG. 5.1. - Isentropic Expansion Velocity Versus Area for Various Stagnation Temperatures (no heat addition).

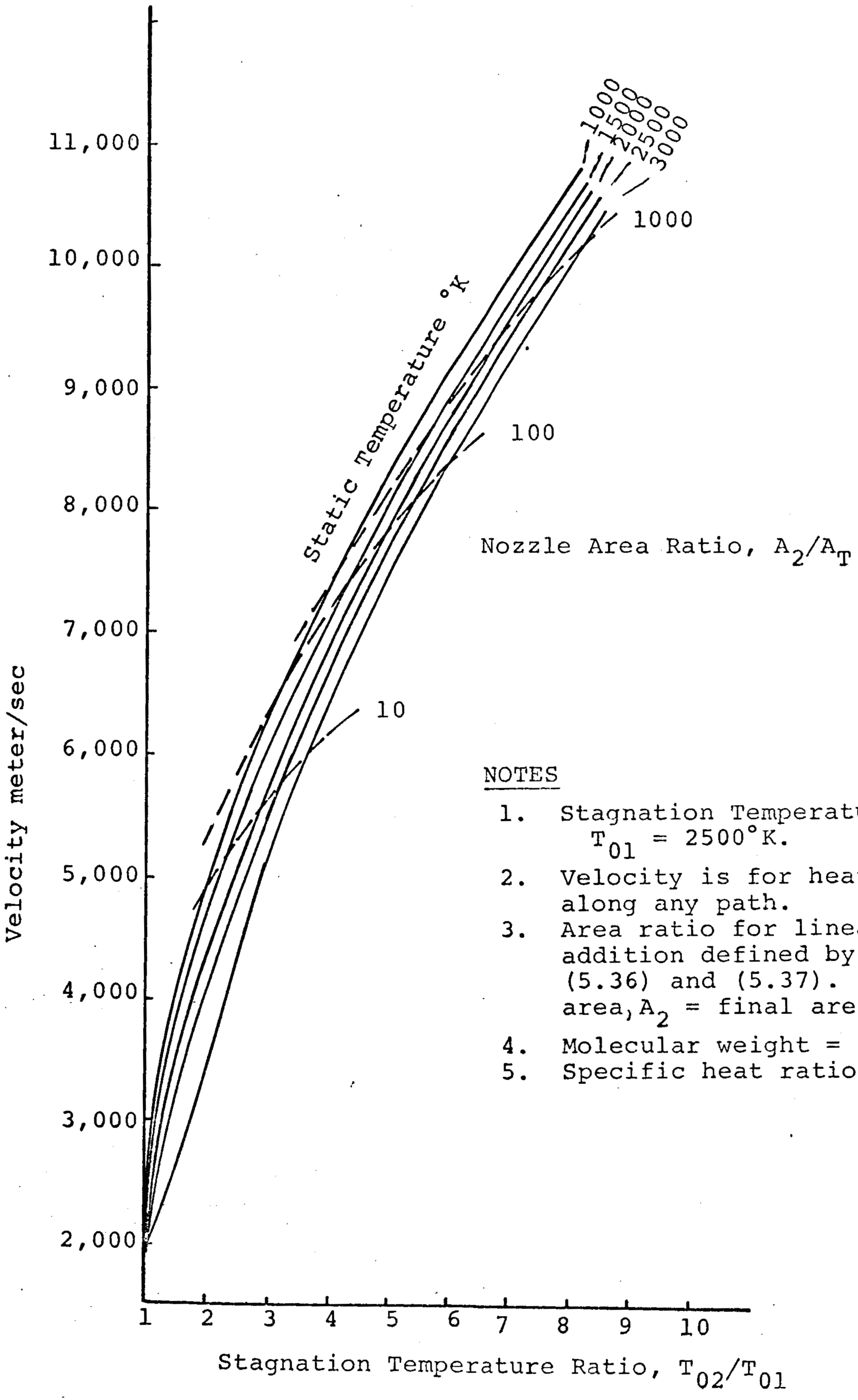

NOTES

1. Stagnation Temperature $T_{01} = 2500°K$.
2. Velocity is for heat addition along any path.
3. Area ratio for linear heat addition defined by Equations (5.36) and (5.37). A_T = throat area, A_2 = final area
4. Molecular weight = 7 (lithium)
5. Specific heat ratio = 1.67

FIG. 5.3. - Velocity Versus Stagnation Temperature Ratio at Various Static Temperatures and Area ratio.

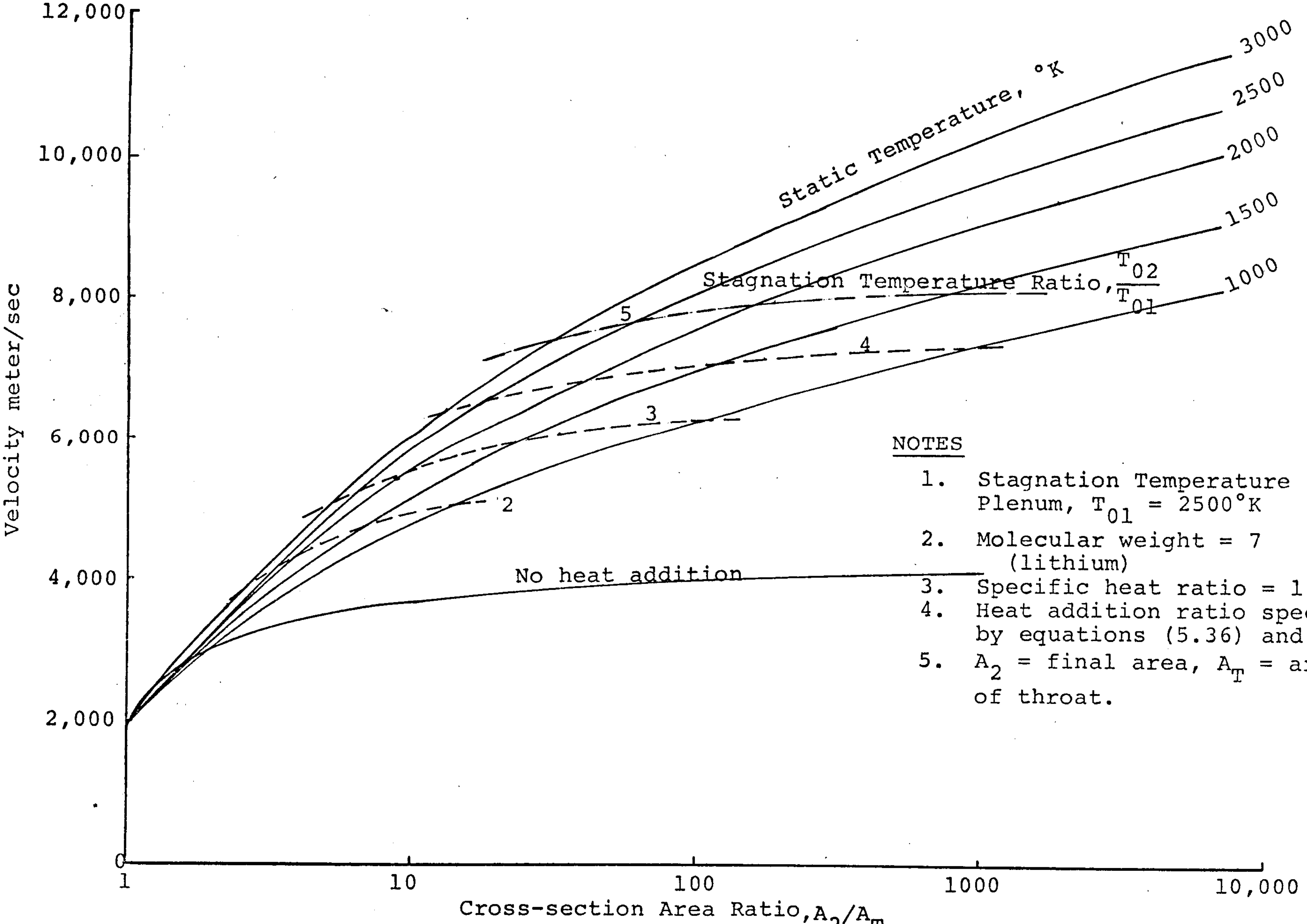

NOTES

1. Stagnation Temperature in Plenum, $T_{01} = 2500°K$
2. Molecular weight = 7 (lithium)
3. Specific heat ratio = 1.67
4. Heat addition ratio specified by equations (5.36) and (5.37)
5. A_2 = final area, A_T = area of throat.

FIG. 5.4. - Velocity Versus Cross Section Area, Static Temperature and Stagnation Temperature Ratio for Linear Heat Addition Path.

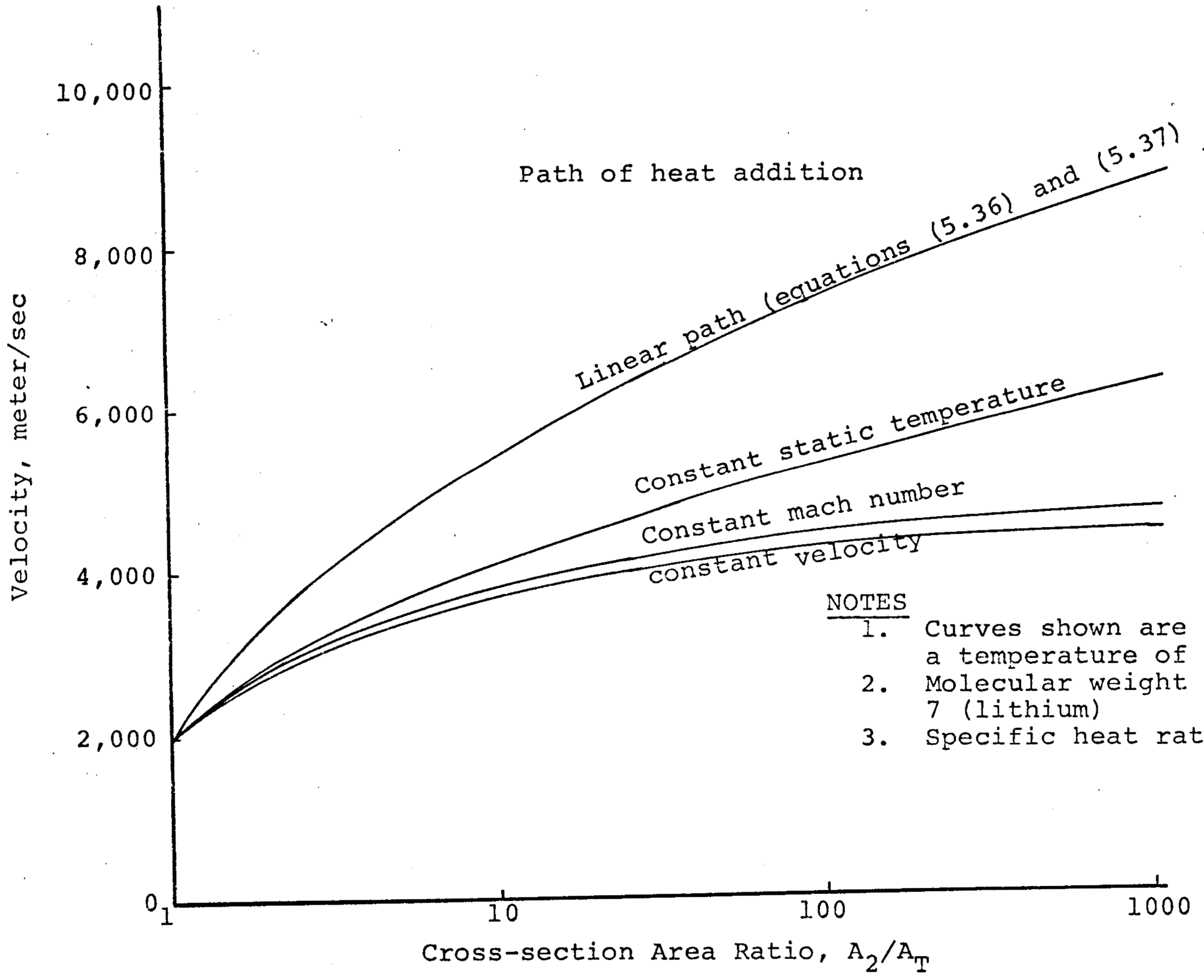

NOTES
1. Curves shown are correlated to a temperature of 1825°K.
2. Molecular weight of gas is 7 (lithium)
3. Specific heat ratio = 1.67

FIG. 5.5. - Velocity Versus Area for Various Paths of Heat Addition.

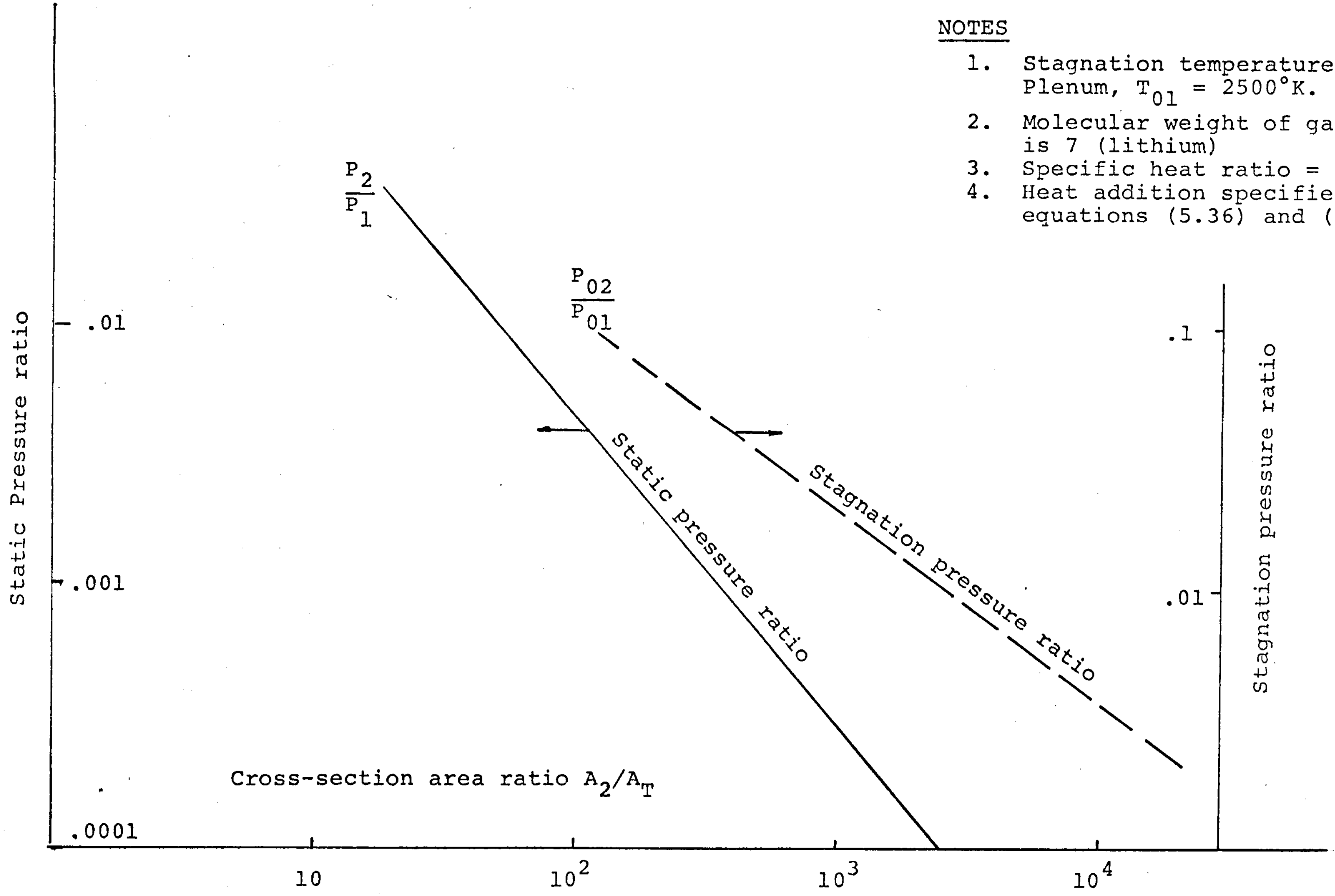

NOTES

1. Stagnation temperature in Plenum, T_{01} = 2500°K.
2. Molecular weight of gas is 7 (lithium)
3. Specific heat ratio = 1.67
4. Heat addition specified by equations (5.36) and (5.37).

FIG. 5.6. - Static and Stagnation Pressure Ratio Versus Area Ratio for Linear Heat Addition.

THE PRODUCTION OF CHARGED COLLOID PARTICLES FROM WASTE-TYPE MATERIALS

by V. Steadman and G. W. Tompkin

The primary goal has been to show by some approximate means that a waste-type material is suitable for use as a propellant in electrostatic colloid thrusters. The particular method chosen for generating the charged colloid particles has been electrohydrodynamic (EHD) spraying. Various properties of a number of materials which were critical in their performance during the EHD spraying process were deduced. Also considered were improvements on the basic EHD spraying apparatus which would extend its range of applicability in charged colloid generation.

The following potential propellants were studied experimentally:

(1) 1.7 g hemoglobin (denatured)/100 ml formamide (with and without heparin additive)*,

(2) 52 g urea/117 g glycerol*,

(3) .0006 M H_2SO_4 (water as solvent),

(4) silver nitrate in glycol-glycerol.

Protein (exemplified by hemoglobin), urea and water are biowastes. Case (4) provided general information on the performance of binary solutions. During electrostatic spraying, the above materials were each subjected to a high potential at a needle tip (here a stainless steel needle with a 90° tip and 8 mil I.D.) into which they were fed under a pressure ranging from 0 cm Hg to 90 cm Hg. At the needle tip, the propellants encountered a vacuum, the pressure of which ranged from 5μ to 200μ. The vacuum varied with the mass flow rate and the vapor pressure of the propellant. The characteristics of the charged particles produced at the needle tip were deduced from their time-of-flight data.

---

* It should be noted in cases (1) and (2) that the concentrations of hemoglobin and of urea, respectively, are not the maximum possible in the given solvents. However, it was found that a three-fold increase in hemoglobin concentration above that in case (1) leads to a gel-forming suspension. The case (1) solution is, however, stable. Glycerol, on the other hand, appears to "dissolve" urea in all proportions upon slight heating.

For the hemoglobin-formamide mixture, a charge-to-mass ratio of 130 coul/kg* was obtained for an applied needle voltage of -3.1 kv, a grounded extractor plane, and a pressure on the feed-line of 3.4 cm Hg. No D.C. current of 0.05 μamp or greater was detectable for any applied needle voltage up to +3.1 kv, however. In Figure 6.1 is shown, from top to bottom, the oscilloscope traces of two superimposed TOF decays and of a baseline accompanying the D.C. current for the hemoglobin-formamide experiment mentioned above. This experiment was run for approximately one-half hour with no appreciable changes in the observed spraying characteristics. However, upon subsequent examination of the needle, a gel-like structure was found to have formed in the needle capillary. An attempt was then made to prevent the gel formation with the addition of heparin to the hemoglobin-formamide mixture. The resultant solution did have a greatly enhanced flow rate for a given pressure on the mass flow line over the non-heparin-doped solution (even when all water was removed from the heparin). But again gel was found to have formed in the needle upon its examination following the experiment. Further, no current of charged particles of .05 μamp or greater was detectable for the heparin-doped solution within the range of needle potentials, ±3 kv.

The urea-glycerol mixture did not give rise to a detectable current of 0.05 μamp or greater for a stainless steel needle such as that described above and for applied needle voltages ranging from -3. kv to +5. kv. Such a result is not surprising since pure glycerine itself would not give rise to a current detectable with a TOF apparatus. (This conclusion is based on the following information: a current of order 1 μμamp is observed for glycerine with the quadrupole mass spectrometer, whereas materials having "total" currents of order 0.05 μamp, give rise to quadrupole mass spectrometer currents or order 100 μμamp.[6.1])

---

* It will be noted that the charge-to-mass ratio observed is dependent upon the size of the TOF collector and its shielding. The q_s given above is somewhat erroneous due to errors arising from these two sources, as well as some difficulty incurred in determining the exact time at which the needle was shorted to ground from the oscilloscope trace. Nevertheless, the TOF trace indicates that charged colloid particles have indeed been formed from a hemoglobin-formamide mixture.

The possibility remains of doping the urea-glycerol mixture with a salt so as to obtain a useful EHD spraying propellant. The mixture already investigated exhibited viscosity and vapor pressure properties similar to those of pure glycerol; these are known from previous investigations to be relatively ideal for a propellant.

The third candidate, water doped so as to be .0006M in sulfuric acid (resistivity estimated from Λ_o is 1920 Ω^{-1} cm^{-1}), has the highest vapor pressure of the three materials tried. To use water, heat must be applied to the needle, especially the needle tip, to prevent the formation of ice, either at the tip or internally. A combination of Joule heating of a wire stuffing of the needle and the focusing of a light beam on the needle provided sufficient heating so that there was a relatively high mass flow of water. In addition, no ice formed at the needle tip. However, the pressure in the system approached atmospheric. A poor vacuum is of course conducive to preventing the formation of ice. Hence the same amount of heating as required in our experiment would not be adequate in the vacuum of space.

Observations on the quantity of and configurations assumed by the ice flows for the H_2SO_4 water propellant tend to agree with previous observations (on $SnCl_4$-glycerol systems 6.2)) that the mass flow of propellant increases with increasing potential on the needle. Among the indications that such is the case were:

1. Ice appears at the needle tip at lower feed-line pressures when a high positive voltage (+2 kv) is applied to the needle than when the needle is grounded.
2. The non-whiskered ice structures characteristic of the high needle potential case for almost all vacuum chamber pressures and feed-line pressures occur for lower needle potentials (+.5 kv) only at feed-line pressures near one atmosphere. (At lower feed-line pressures, the lower needle potential gives rise to ice structures which are multi-whiskered.)

The above results indicate that the rate of evaporation at needle tips during EHD spraying dominates over the rate of charged colloid formation for high vapor pressure solutions. (Even for very low vapor pressure propellants, the two rates are competitive since there is a 23% mass loss at the needle tip for doped glycerol.[6.3)] Processes occurring at vacuum interfaces for high vapor pressure solutions of proteins and of other large molecules should then be expected to occur at a needle tip, almost irregardless of the potential applied thereon. Gel formation is the ordinary result of the exposure of a hemoglobin-formamide solution to even a low vacuum.* (If the vacuum and vapor pressure of the solvent are sufficiently high, then freezing of the solution may be expected instead.)

There thus appear to be two alternatives remaining if one wishes to spray large molecules electrostatically:

1. Utilize very low vapor pressure solvents. (Such solvents were not utilized in the case of proteins because they do not solvate proteins.)
2. Hydrolyze the proteins into their amino acid subunits. (The solvent of lowest vapor pressure may again be formamide. Gel formation at vacuum interfaces in the case of the amino acids is not anticipated.)

The performance of formamide as a propellant is however non-ideal. The possibility exists though of forming charged particles from amino acids in binary solutions, the higher vapor pressure component of which is formamide. But what results may be expected from binary solutions in general? Greater evaporation of the higher vapor pressure component will undoubtedly occur; probably the characteristics of the particles produced in electrostatic spraying will be similar to those occurring in the pure (but suitably doped) lower vapor pressure component. Our preliminary results on glycerol, a 50-50 mixture of glycerine and glycol, and glycol (doped with 8g silver nitrate/50ml solvent) indicated that the situation is more complex. EHD spraying is possible at both negative and positive potentials (below 3 kv in magnitude) for doped glycerol alone; but, within the same range, EHD spraying is possible only for negative potentials for the doped glycerol-glycol and doped glycol solutions.

---

* The tendency toward gel formation is particularly aggrevated in the case of proteins because these highly structured molecules unfold under reduced pressure.

One would like to think that the foregoing indicates that solutes which are soluble only in the higher vapor pressure component might not necessarily build up in the needle capillary during EHD spraying. However, the occurence of such a phenomenon in EHD spraying probably requires a considerable degree of binding of the solute to the higher vapor pressure component. Complexation might be necessary--as is indicated to be present in the silver nitrate-glycol mixture from the analysis below. Because of the large effect observed in the case of complexation, it may nevertheless be possible to correlate EHD spraying characteristics with the much weaker ion-solvent or amino acid-solvent interactions.

Glycol and glycerol appear to be, at first glance, very similar alcohols having chemical formulas

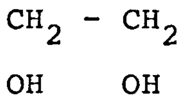

$$\underset{OH}{CH_2} - \underset{OH}{CH_2}$$

(glycol)

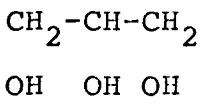

$$\underset{OH}{CH_2}-\underset{OH}{CH}-\underset{OH}{CH_2}$$

(glycerol)

However, significantly more intermolecular hydrogen-bonding must occur in the pure glycerol solution. This higher degree of hydrogen-bonding probably presents the silver ion from forming a complex with glycerol. The silver ion apparently does combine by complexation with less highly hydrogen-bonded glycol. The silver ion in glycol, but not in glycerine, is in some state energetically unfavorable for the expulsion of positive colloid particles from the capillary liquid surface. (The nitrate ion is presumably equally mobile and capable of neutralization at the capillary surface for the various glycerol and glycol solutions. Hence nitrate ion is not the major source of difficulty in EHD spraying at positive potentials for those glycol-containing systems.) If silver ion is indeed complexed in glycol solutions but not in glycerol alone, one wonders whether greater energy would be required to neutralize the complexed silver ion at the capillary surface than in its uncomplexed state. (Changes in neutralization energy have been correlated with the failure of certain systems to spray electrohydrodynamically.) Complexation should lower the ground-state energy level of silver ion in solution, thereby increasing the probability of electron tunneling from the capillary surface for a given negative needle potential. But the closer association of the "solvent" in complexation will also hinder electron tunneling. Further, the reduced conductivity of the complexed silver ion as it moves toward the capillary surface for neutralization should require an increase in capillary potential to affect a given q/m[1] or the critical spraying potential itself. Our initial results indicate that these opposing effects may cancel, since the critical potential at which spraying commenced (for a given needle) was approximately the same throughout the three doped glycol and glycerol solutions. (Also the critical potential was approximately the same in magnitude for both the positive and the negative critical spraying potentials in the glycerine case--±2.4 kv.) A tentative conclusion is that the reduced speed of migration of the complexed silver ion to the liquid surface has caused the failure of doped glycol solutions to spray electrostatically at positive potentials below 3 kv. In agreement with this idea is the fact that complexation greatly reduces the conductivity of ions.

An understanding of the role of solvent-solute attractions in general will enable one to select materials judiciously for use in charged colloid generation by EHD spraying. The importance of such interactions is evident not only from the complexation case above but also from peculiar conductivity effects. The absolute value of the conductivity of a given solution appears to be of lesser importance in determining the EHD spraying characteristics of the solution than are the structure of the solution and the relative positions of the counterions immediately surrounding a given ion. Previous work[6.2] has shown, in the cases of $FeCl_3$ and $SnCl_4$ in glycerol, that the increase in conductivity accompanying an increase in temperature for a given solution does not alter q/m for a fixed needle potential and mass flow rate. (The mass flow rate was measured by the TOF collector. The mass flow rate is a function of the temperature, but it can also be increased by application of increased pressure on the feed-line without altering the conductivity.)

Such a result disagrees with Pfeifer's expression for the dependence of q/m on the conductivity $\sigma(E_o)$:

$$\frac{q}{m} \simeq \left[\left(\frac{4\pi}{\varepsilon}\right)^2 (9\delta)^2 \frac{E_o^5}{\rho^4} \right]^{1/7} \left(\frac{\sigma(E_o) E_o}{\dot{M}} \right)^{3/7}$$

where $\dot{M}$ = mass flow rate
δ = surface tention
ρ = density
E_o = electric field strength at the capillary tip.

However, for glycerine doped with NaCl, the dependence of q/m on $\sigma(E_o)$ is such that quite distinctive curves of σ as a function of E_o are closely paralleled by curves of q/m as a function of E_o.[6.4] The difference in the conductivity effects in the two experiments may lie in the fact that an electric field tends to asymmetrize the distribution of counterions about a given ion, whereas increases in temperature tend to smear out the ion cloud by relaxation effects.

Such a dependence on microscopic structure in EHD spraying does not seem unreasonable when one considers that such spraying occurs in jets. These jets are relatively highly stable in direction and content, though the content varies considerably from one jet to the next. This phenomenon of stable jets with different contents leads one to think the liquid might be structured with definite routes (some distance back from the liquid meniscus) through which a given ionic species can travel. In the case of pure dielectrics, it is known that space charge distorts the field so that at field strengths near breakdown, electrical conduction tends to occur in filaments.[6.5] A similar phenomenon may occur at the needle tip in doped dielectrics, though at field strength considerably below the dielectric breakdown potential.

In all, the phenomenon of EHD spraying in general will be more comprehensible when various distinctions due to microscopic variations in conductivity are incorporated into the theory. The quadrupole mass spectrometer or a modified TOF spectrometer which analyzes only one jet at a time should provide more precise information on the effects of these microscopic differences.

6.1. Cohen, E.: Research on Charged Colloid Generation. APL TDR 64-75, June 1964. Wineland, S. H., Burson, W. C., and Hunter, R. E.: The Electrohydrodynamic Generation of Charged Droplet Beams, AFAPL-TR-66-72, 1966.

6.2. Kidd, P. W.: Parametric Studies of a Single Needle Colloid Thruster, AIAA Paper No. 67-530 (1967).

6.3. Notes on paper given by M. N. Huberman at the AIAA Electric Propulsion and Plasmadynamics Conference, Colorado Springs, Colorado, September, 1967.

6.4. Hendricks, C. D., and Pfeifer, R. J.: Parametric Studies of Electrohydrodynamic Spraying. AIAA Paper No. 66-252 (1966).

6.5. Goodwin, D. W.: "Space Charge Phenomena in Liquid Dielectrics," Proc. Phys. Soc. London, 69B, 61 (1956).

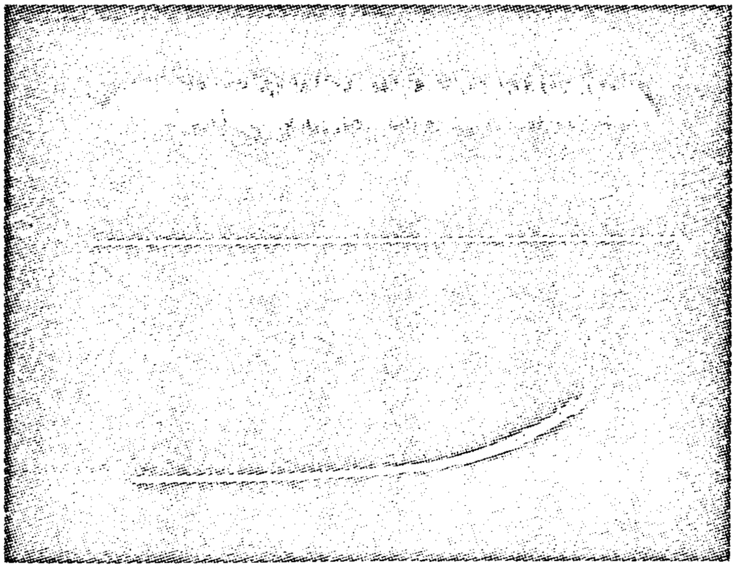

FIG. 6.1. - TOF Oscilloscope Trace (upper) and the D.C. Current Trace (lower) for the Hemoglobin-Formamide Mixture.

Colorado State University

ERRATA for

ANNUAL REPORT

For the period January 1, 1967 to December 31, 1967

ADVANCED ELECTRIC PROPULSION RESEARCH

Prepared for

NATIONAL AERONAUTICS AND SPACE ADMINISTRATION

December 1967

Grant NGR06-002-032

---

page 3.5, last sentence in first paragraph should read:

"In other words, mercury bombardment thrusters will always have about 2.5 times the discharge power loss of cesium bombardment thrusters."

---

page 4.2, third sentence in first paragraph should read:

Too much power would be lost in the original gear drive, and

---

page 5.10, equation (5.21a) should read:

$$\frac{T_{02}}{T_{01}} = \frac{T_2 + V_2^{\,2}/2C_p}{T_1 + V_1^{\,2}/2C_p} \qquad (5.21a)$$

---

page 5.11, equation (5.21b) should read:

$$\frac{T_{02}}{T_{01}} = \frac{T_2 + B}{T_1 + B} \qquad (5.21b)$$

---

page 6.7, fifth line from top should read:

δ = surface tension

---

page 6.8. Figure 6.1 was mounted upside down.

February 2, 1968